Inorganic Chemistry

pubs.acs.org/IC Article

Revealing the Structure of Transition Metal Complexes of Formaldoxime

Ivan S. Golovanov, Roman S. Malykhin, Vladislav K. Lesnikov, Yulia V. Nelyubina, Valentin V. Novikov, Kirill V. Frolov, Andrey I. Stadnichenko, Evgeny V. Tretyakov, Sema L. Ioffe, and Alexey Yu. Sukhorukov*

Cite This: *Inorg. Chem.* 2021, 60, 5523−5537 Read Online

ACCESS | Metrics & More | Article Recommendations | Supporting Information

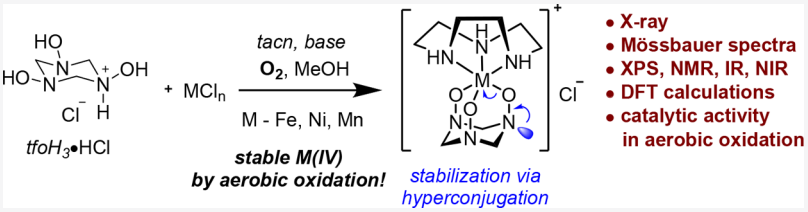

ABSTRACT: Aerobic reactions of iron(III), nickel(II), and manganese(II) chlorides with formaldoxime cyclotrimer ($tfoH_3$) and 1,4,7-triazacyclononane (tacn) produce indefinitely stable complexes of general formula [M(tacn)(tfo)]Cl. Although the formation of formaldoxime complexes has been known since the end of 19th century and applied in spectrophotometric determination of d-metals (formaldoxime method), the structure of these coordination compounds remained elusive until now. According to the X-ray analysis, $[M(tacn)(tfo)]^+$ cation has a distorted adamantane-like structure with the metal ion being coordinated by three oxygen atoms of deprotonated $tfoH_3$ ligand. The metal has a formal +4 oxidation state, which is atypical for organic complexes of iron and nickel. Electronic structure of $[M(tacn)(tfo)]^+$ cations was studied by XPS, NMR, cyclic (CV) and differential pulse (DPV) voltammetries, Mössbauer spectroscopy, and DFT calculations. Unusual stabilization of high-valent metal ion by tfo^{3-} ligand was explained by the donation of electron density from the nitrogen atom to the antibonding orbital of the metal−oxygen bond via hyperconjugation as confirmed by the NBO analysis. All complexes [M(tacn)(tfo)]Cl exhibited high catalytic activity in the aerobic dehydrogenative dimerization of *p*-thiocresol under ambient conditions.

INTRODUCTION

In 1898, Dunstan and Bossi[1] observed that formaldehyde oxime ($H_2C{=}NOH$) forms intensively dark-colored species upon reaction with transition metal salts (Mn, Fe, Ni, Cu) in alkaline solutions. In 1913, Hofmann and Ehrhardt[2] succeeded in isolating some of these species, in particular manganese, iron, and nickel complexes, for which chemical formulas $Mn(ONCH_2)_3$, $Na_2Fe(ONCH_2)_5$, and $Na_3Ni(ONCH_2)_6$ were proposed based on elemental analysis. These authors disclosed that oxygen was required to form these complexes in order to oxidize the metal ion. In the reaction with formaldoxime or its cyclotrimer $tfoH_3$, manganese gave the most intensive coloring, which allowed the analytical determination of this metal at very low concentrations.[3−5] Since then, the formaldoxime method has become one of the most reliable techniques for colorimetric or spectrophotometric determination of manganese in the presence of other metals.[6−11] Moreover, the use of formaldehyde oxime as an effective extracting agent of d-metals from several types of ores, such as pyrolusite, malachite, heterogenite, and deep-sea manganese nodules, was suggested.[12]

Given the unusual composition of metal-formaldoxime complexes and their use in analytical chemistry and extraction, numerous studies were performed to establish their structure. In the 1960s, the composition of the metal-formaldoxime anion was revised to $[M(ON{=}CH_2)_6]^{2-}$,[13−15] which was shown to be general at least for M = Mn, Fe, Ni, V, and Ce (Scheme 1a).[16] Several metal-formaldoxime complexes were isolated and characterized by elemental analysis, UV−vis, IR spectra, and electrochemical methods.[13−15] However, the structure of the $[M(ON{=}CH_2)_6]^{2-}$ dianion and related metal-formaldoxime species was a matter of debate (Scheme 1b), and surprisingly, it was not determined yet.[15,17−19]

In this paper, we succeeded in the preparation and full structural characterization (X-ray, HRMS, NMR, IR, Raman,

Received: November 12, 2020
Published: April 7, 2021

https://doi.org/10.1021/acs.inorgchem.0c03362
Inorg. Chem. 2021, 60, 5523−5537

Scheme 1. Metal-Formaldoxime Complexes: Background

a. Formation of metal-formaldoxime complexes

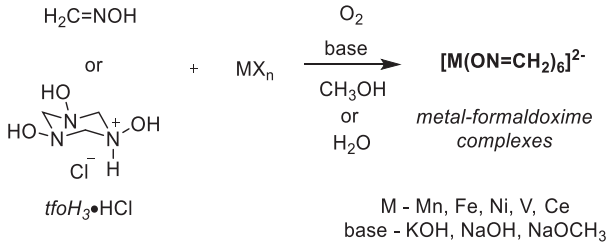

b. Plaussible structures of metal-formaldoxime complexes

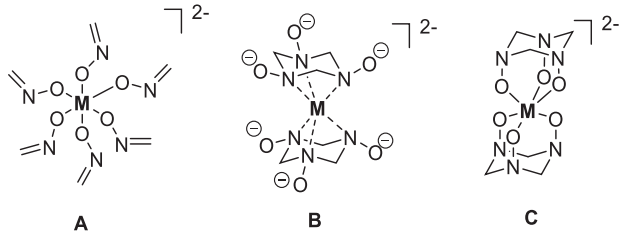

c. Reversible trimerization of formaldoxime to tfoH3

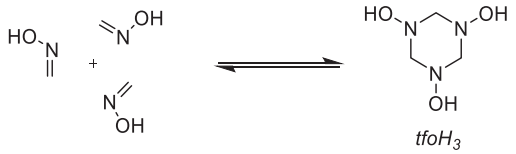

XPS, and Mössbauer spectroscopy) of closely related complexes $[M(ONCH_2)_3L]^+Hal^-$ (L, neutral polycyclic triamine) derived from manganese, iron, and nickel. These experimental studies together with high-level DFT calculations provide insights into the structure of metal-formaldoxime complexes, which have been known for more than 120 years. Our results also provide background for the design of structurally well-defined high-valent d-metal complexes for applications in analytical chemistry and aerobic oxidation catalysis.

RESULTS AND DISCUSSION

Three possible constitutional isomers shown in Scheme 1b have been proposed for the dianion $[M(ON{=}CH_2)_6]^{2-}$.[17−19] In structure A, the metal ion is coordinated by six formaldoxime anions. In the other two structures B and C, the deprotonated cyclic trimer of formaldoxime serves as a ligand through coordination with nitrogen or oxygen atoms. Moreover, isomeric structures with mixed coordination modes of the ligand cannot be ruled out. In most of the literature, structure A is postulated, yet some evidence in support of structures B[18] and C[19] was obtained from IR spectra.

A remarkable experimental observation is that $[M(ON{=}CH_2)_6]^{2-}$ complexes are formed only with formaldoxime, while substituted oximes (even acetaldehyde oxime) are inert. Recently, when studying the complexation of oximes with boronic acids,[20] we have shown that substituted oximes do not undergo reversible cyclotrimerization as readily as formaldoxime does.[20] Furthermore, with formaldoxime trimer $tfoH_3$ (taken in the form of stable hydrochloride salt $tfoH_3{\cdot}HCl$), the same metal complexes are formed as with formaldoxime.[13] On the basis of these experimental facts, we concluded that structure A is unlikely, and metal-formaldoxime complexes might possess a hexahydrotriazinane ring as the ligand. This was confirmed by DFT calculations at the DFT-D3 BP86/jorge-atzp level of theory, which predicted structure C to be more stable than A and B by 58.2 and 79.6 kcal/mol, respectively (for M = Fe, see Supporting Information).

Synthesis of Formaldoxime Complexes. To verify this hypothesis, we generated several metal-formaldoxime complexes $Na_2[M(ON{=}CH_2)_6]$ (M = Mn, Fe, Ni) following the procedures of Okáč and Bartušek[13] and Andersen and Jensen[17] from $tfoH_3{\cdot}HCl$ or formaldoxime. However, these compounds proved to be amorphous solids, which underwent decomposition to form insoluble material upon attempts to prepare suitable crystals for X-ray analysis. Our attempts to get crystalline complexes $Cat_2[M(ON{=}CH_2)_6]$ containing organic cations derived from amine bases (Et_3N, py) were also not successful. Moreover, in the reaction of $FeCl_3$ with $tfoH_3{\cdot}HCl$ and pyridine (*py*), a blue complex $Fe(ON{=}CHNO)_2py_2$ (**1**) was isolated in a small yield (Scheme 2).

Scheme 2. Formation of Iron(II) Nitrosolate Complex 1

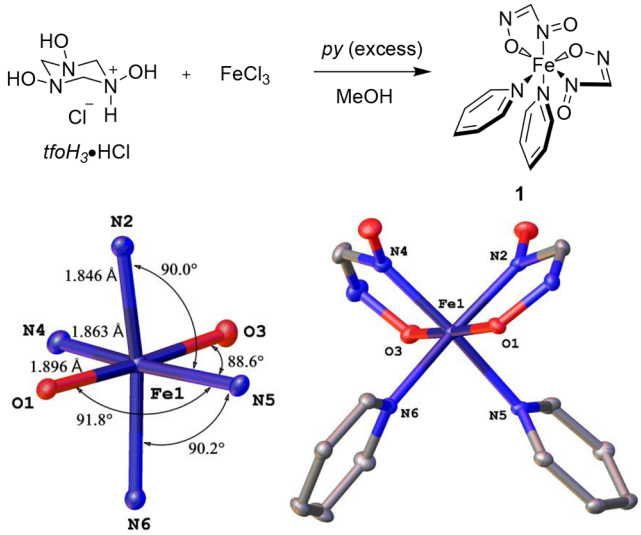

According to the X-ray analysis of complex **1**, iron(II) was coordinated by two deprotonated nitrosoformaldoximes (nitrosolate anions[21]) and two pyridine molecules. The formation of nitrosolate complexes in reactions of formaldoxime or $tfoH_3$ with transition metals was never observed previously. Interestingly, $tfoH_3$ or formaldoxime are not oxidized to nitrosoformaldoxime with O_2, suggesting that an iron-promoted process may take place.

Since the lability of $[M(ON{=}CH_2)_6]^{2-}$ complexes could be attributed to the formation of oligomeric and polymeric species, we reasoned that substitution of three formaldoxime anions for a tripodal capping ligand could result in stabilization of the complex. To test this idea, 1,4,7-triazacyclononane (tacn) was used as a capping ligand. We were happy to find that the reaction of $Na_2[Fe(ON{=}CH_2)_6]$ with tacn·3HCl in methanol afforded an isolable deep violet crystalline complex $[Fe(tacn)(ONCH_2)_3]Cl$ (**2**, Scheme 3).

https://doi.org/10.1021/acs.inorgchem.0c03362
Inorg. Chem. 2021, 60, 5523−5537

Scheme 3. Synthesis of Iron(IV)-tfo Complex [Fe(tacn)(tfo)]Cl (2)

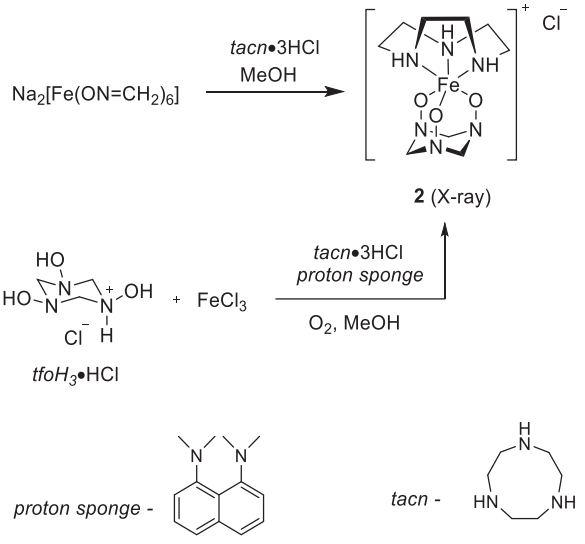

The same complex was prepared in 42% yield directly from $FeCl_3$ by the reaction with hydrochlorides of tacn and $tfoH_3$ in the presence of a proton sponge (1,8-bis(dimethylamino)-naphthalene) under air. The use of formaldoxime (generated *in situ* from formaldehyde and hydroxylamine) instead of its trimer $tfoH_3$ in this reaction led to the same result. The composition of complex **2** was proved by HRMS (electrospray ionization) and elemental analysis. UV−vis and FT-IR spectra of **2** were similar to those reported previously for $Cs_2[Fe(ON{=}CH_2)_6]$ (see the Supporting Information), indicating the presence of the same structural motif in these two complexes. For crystals of complex **2**, the X-ray analysis could be performed, which revealed that the iron atom is coordinated not by formaldoxime (as postulated previously) but by its trimer (tfo). The N−OH groups of the ligand are fully deprotonated, and oxy groups are bonded to iron forming an adamantane-like structure $[Fe(tacn)(tfo)]^+$. Intriguingly, the formal oxidation state of iron is +4 in this complex, assuming that tfo ligand is a trianion (*vide infra*).

Inspired by this result, we then tried to prepare mixed tfo-tacn complexes with other D-metals. However, attempts to isolate tfo-tacn complexes with cobalt, copper and vanadium failed.[22] Surprisingly, the reaction of $NiCl_2$ with tacn and $tfoH_3$ hydrochlorides in the presence of a proton sponge in methanol under air afforded a stable brown-colored nickel complex [Ni(tacn)(tfo)]Cl·MeOH (**3**, Scheme 4). According to the X-ray analysis, this complex had the same metalloadamantane motif (nickel coordinated by three *N*-oxy groups of tfo^{3-}) as the parent iron complex **2**.

Scheme 4. Synthesis of Nickel(IV)-tfo Complex [Ni(tacn)(tfo)]Cl·MeOH (3)

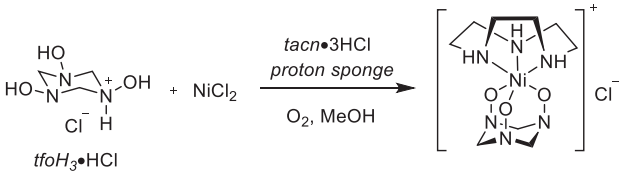

In a similar fashion, an intensively wine-colored manganese complex [Mn(tacn)(tfo)]Cl (**4**) was prepared from $Mn(OAc)_3$ or $MnCl_2$ under air. The composition of **4** was established on the basis of HRMS and elemental analysis. Although the crystals were of poor quality, the X-ray analysis showed that the manganese ion is coordinated by three oxygen atoms of formaldoxime trimer as in the corresponding iron and nickel complexes **2** and **3**. Attempts to get better crystals by the metathesis of the anion were not successful. We, therefore, tried to use other tripodal N^3-ligands (1,3,5-trimethyl-1,3,5-triazacyclohexane, 1,4,7-triazacyclononane, 1,5,9-triazacyclododecane, trispyrazolylborate).[23] Finally, we were able to get a good quality X-ray structure by using the *N*,*N*′,*N*″-trimethyl-1,4,7-triazacyclononane (Me_3tacn) as a capping ligand (complex **5**, Scheme 5).

Scheme 5. Synthesis of Manganese(IV)-tfo Complexes [Mn(tacn)(tfo)]Cl (4) and [Mn(Me_3tacn)(tfo)]Cl·MeOH (5)

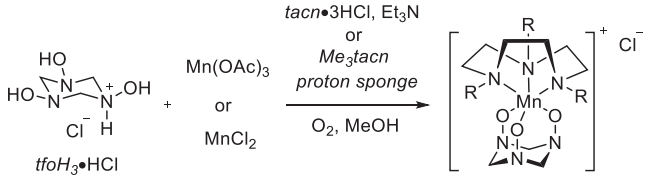

It is noteworthy that metal(IV)-tfo complexes were not formed under the argon atmosphere, indicating that oxygen is required for the oxidation (*vide infra*).

The obtained metal-tfo complexes **2**−**5** are well-soluble in methanol, water, and DMF and poorly soluble in Et_2O, THF, and CH_2Cl_2.

X-ray Structure of Metal-tfo Complexes, FT-IR and NIR Spectroscopy. The geometry and electronic structure of complexes **2**−**5** are unprecedented and require special discussion. It is surprising that at least three D-metals with different electronic configurations tend to form stable complex cations of the same composition $[M(tacn)(tfo)]^+$ with a formal +4 oxidation state of the metal. Stable nonbiomimetic high-valent iron(IV)[24−31] and nickel(IV)[32−38] complexes with organic ligands are scarcely known in the literature. Moreover, the formation of high-valent nickel and iron species by oxidation with molecular oxygen is extremely rare.[24,31] To our knowledge, compounds **2** and **3** are the first structurally characterized organic nitroxy complexes of iron(IV) and nickel(IV), which are formed under ambient conditions by a spontaneous oxidation with air. Somewhat related iron(IV) complexes with macrocyclic amides such as TAMLs[28−30] and hexahydrazide cages[24] have been reported in the literature. However, these complexes are stabilized by donor effects of deprotonated amides as well as by a shielding effect of clathrochelate,[24] which is not the case in tfo complexes.

The geometrical parameters of $[M(tacn)(tfo)]^+$ cations are very similar for manganese, iron, and nickel (Figure 1). All three structures consist of a distorted metalloadamantane framework formed by coordination of the metal ion with three axial (with respect to triazinane ring) oxy groups of the deprotonated $tfoH_3$ ligand. The other three coordination

https://doi.org/10.1021/acs.inorgchem.0c03362
Inorg. Chem. 2021, 60, 5523−5537

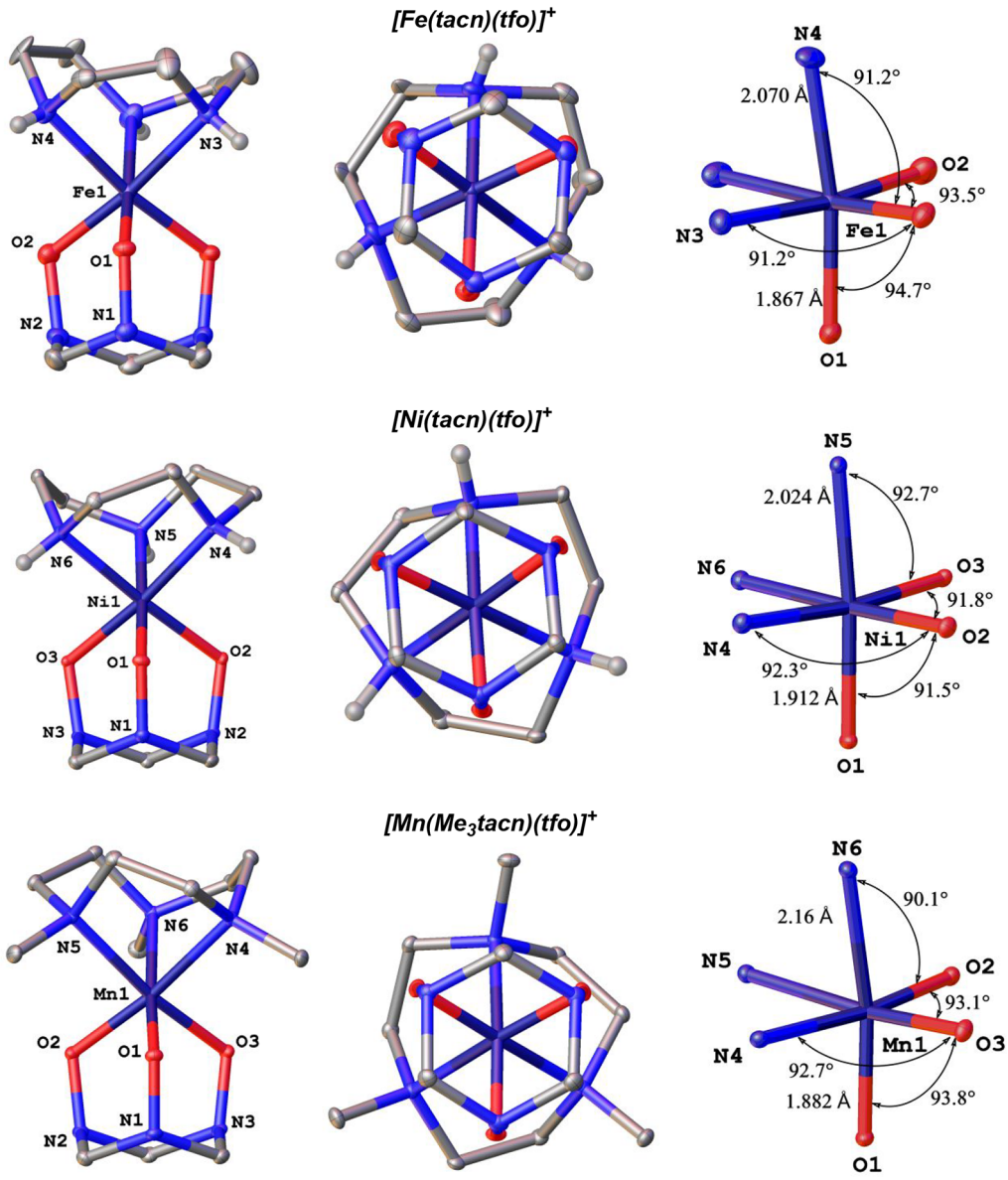

Figure 1. Principal structural motifs and details of geometries around a metal center in complexes **2**, **3**, and **5**. Hydrogens at carbon atoms are omitted for clarity.

vacancies on the metal are occupied by the triazacyclononane ligand (tacn or Me_3tacn). The coordination geometry around the metal ion is close to an ideal octahedron, as follows from the angles of distortion toward a trigonal prism in the range 49.41(4)−51.54(10) (φ = 0° for an ideal trigonal prism, φ = 60° for an ideal octahedron). To better quantify this distortion, continuous symmetry measures were used[39] that measure how close the shape of the coordination polyhedron is to a reference shape, such as an ideal octahedron (OC) and an ideal trigonal prism (ITP). For all the complexes synthesized, the symmetry measures S(OC) and S(TPR) evaluated from the X-ray diffraction data confirm a very small deviation of the shape of the coordination polyhedron from an ideal octahedron hinted by the above distortion angles (Table 1).

The M−O and N−O bond distances in iron and manganese complexes are close and lie in the range of 1.86−1.89 Å and 1.39−1.41 Å, respectively. In [Ni(tacn)(tfo)]$^+$, the Ni−O bonds are somewhat longer (1.909−1.917 Å), and N−O bonds are considerably shorter (1.345−1.352 Å) compared to manganese and iron complexes. Axial N−O bonds in the ligand are longer (1.455 Å) compared to metal-tfo complexes as shown by X-ray analysis of $tfoH_3$·HCl. Remarkable features of all three structures are reduced pyramidality of nitrogen atoms (deviation of nitrogen from

Table 1. Main Geometric Parameters and Continuous Symmetry Measures[a] As Obtained from X-ray Diffraction at 120 K for 2, 3, and 5

	2	3	5
ϕ (deg)	50.91(17)	51.54(10)	49.41(4)
h (Å)	2.3353(3)	2.3435(12)	2.4339(10)
S(OC)	0.172	0.100	0.295
S(TPR)	16.185	15.784	14.847

[a] φ is the distortion angle of the OC-TPR polyhedron, h is the height of this polyhedron; S(OC) and S(TPR) are octahedral and trigonal prismatic measures, respectively.

https://doi.org/10.1021/acs.inorgchem.0c03362
Inorg. Chem. 2021, 60, 5523−5537

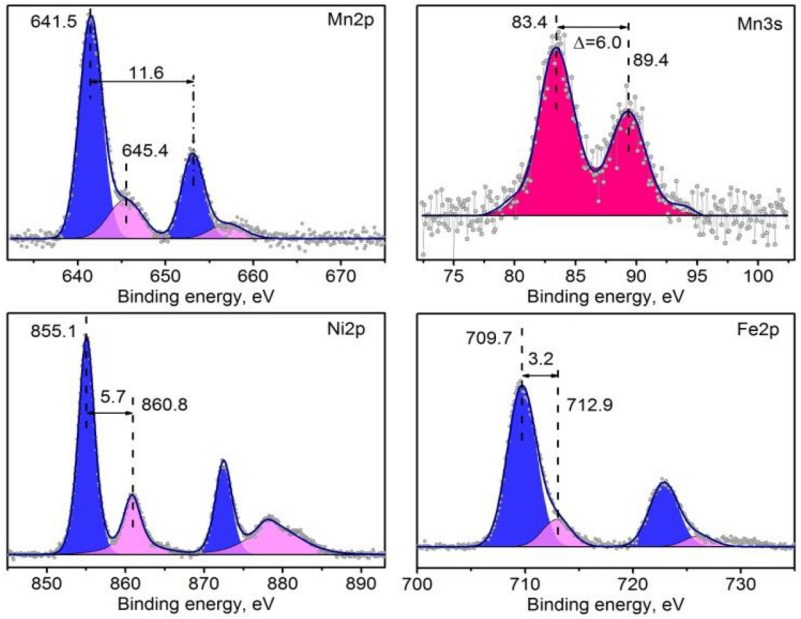

Figure 2. Curve fitted Mn 2p, Mn 3s, Ni 2p, and Fe 2p photoelectron lines for metal-tfo complexes **2**, **3**, and **5** (colored peaks show deconvolution of the experimental spectra on individual components).

the mean plane formed by substituents is ca. 0.4 Å) and shortening of N−O bonds compared to noncoordinated derivatives of $tfoH_3$ (1.42−1.47 Å[40−42]). These features are usually an indication of hyperconjugation interactions involving a lone electron pair ($n \rightarrow \sigma^*$ donation, *vide infra*).[43] Reduced pyramidality of nitrogen atoms in these structures can also be explained by the distortion of bond angles C−N−O attributed to the presence of a large D-metal in the adamantane cage.

FT-IR spectra of $[M(tacn)(tfo)]^+$ complexes display similar features. Characteristic bands attributed to CH_2 stretching, CH_2 bending, CH_2 twisting, C−N−C stretching, N−C−N bending, and M−O stretching were observed. In all spectra, two bands appearing at ca. 1010−920 cm^{-1} are the most intensive. On the basis of the isotope frequency shifts in complexes having ^{15}N-labeled and deuterated tfo ligands, DFT calculations, and previous IR studies on $[M(ON{=}CH_2)_6]^{2-}$ complexes,[19] the higher-frequency band was attributed to an almost pure N−O stretching, while the lower one corresponds to CH_2 rocking (see Tables S4−S6 in the Supporting Information). The position of ν(N−O) stretching frequency is characteristic for a single nitrogen−oxygen bond observed in hydroxylamanines[44] and metal hydroxamates[45−47] (1100−900 cm^{-1}). In the NIR region (1100−2000 nm), no charge transfer bands were observed.

NMR Spectroscopy and Evans Method. The low-spin nature of the nickel(IV) complex with a d^6 electronic configuration was confirmed by its diamagnetic NMR spectra. ^1H and ^{13}C NMR spectra show clear signals of coordinated tfo and tacn having diastereotopic CH_2−protons. In contrast, the NMR spectra of iron and manganese complexes were dominated by the paramagnetic effects (see section 7 in Supporting Information), i.e., the contact shifts that depend on the spin density distribution in a molecule and the pseudocontact shifts that arise from dipole−dipole electron−nucleus interactions. While a full assignment of these signals is outside the scope of this manuscript, the signals being relatively narrow even for the manganese complex are indicative of the spin density being mostly localized on the metal ion, thus ruling out the existence of the nitroxide radical moiety in the molecule.

The magnetic susceptibilities χT of the iron and manganese complexes (1.2 and 1.9 $cm^3{\cdot}mol{\cdot}K^{-1}$ respectively) estimated by the Evans method[48] (see Table S3 in Supporting Information), often used for this purpose, are close to spin-only values for $S = 1$ and $S = 3/2$ (1.00 and 1.87, respectively). This corresponds to two unpaired electrons for a d^4 configuration of the iron(IV) ion and to three unpaired electrons for a d^3 configuration of the manganese(IV) ion, thus confirming the oxidation state of +4 for the metal ions for both paramagnetic complexes.

XPS, Mössbauer Spectroscopy, and DFT Studies of Metal-tfo Complexes. Additionally, the electronic structure of [M(tacn)(tfo)]Cl complexes was studied by X-ray photoelectron spectroscopy (XPS), Mössbauer spectroscopy, and DFT calculations. XPS data confirmed the composition of complexes **2**, **3**, and **5** and the presence of key structural motifs (see Supporting Information). XP spectra with respect to the metal 2p and 3s regions are shown in Figure 2. In all complexes, the metal atom is present in a single oxidation state; i.e., the samples were redox pure. Although there is not much XPS data for high-valent metal complexes with organic ligands,[49] some evidence on the metal oxidation state can still be obtained. For complex **5**, the binding energy at maximum peak height Mn $2p_{3/2}$, doublet splitting ($2p_{3/2}-2p_{1/2}$ = 11.6 eV), and the position and intensity (27% of Mp2p main line) of satellite peaks are consistent with known high-valent manganese complexes, in particular, Mn(IV) complexes with amino alcohol ligands,[50] $Ni[Mn(CN)_6]$,[51] and $K_3[Mn(CN)_6)]$,[51] as well as with some Mn(III) complexes such as β-diketonates.[52] The position of Mn 3s peaks is intermediate between Mn(IV) and Mn(III) complexes with N,O ligands.[49,53] For nickel complex **3**, the positions of main and satellite peaks in the Ni 2p XPS spectrum are very similar to $KNiIO_6$ (855.4, 861.1, 873.0, 880.2 eV[54]), in which Ni(IV) has an octahedral environment and the Ni−O bond

https://doi.org/10.1021/acs.inorgchem.0c03362
Inorg. Chem. 2021, 60, 5523−5537

length (1.88 Å) is close to [Ni(tacn)(tfo)]Cl. The observed $2p_{3/2}$ binding energy values are somewhat smaller than those reported for other high-valent inorganic compounds of nickel, such as K_2NiF_6 and Ni_2O_3.[49] The Fe 2p XPS spectrum of [Fe(tacn)(tfo)]Cl is more consistent with inorganic Fe(III) compounds.[49,55] However, the electronic effect of the organic ligand is known to influence the binding energy state of the electron significantly by changing the effective charge on the metal atom.[56] Thus, a direct comparison of XPS data for iron and nickel tfo complexes with high-valent inorganic compounds of these metals may not be reliable for interpreting the oxidation state.

For iron complexes, Mössbauer spectra are more informative and reliable in interpreting the metal oxidation state. The ^{57}Fe Mössbauer spectrum of [Fe(tacn)(tfo)]Cl (**2**) shows a quadrupole doublet with an isomer shift δ = 0.155(1) mm/s and a quadrupole splitting $|\Delta E_Q|$ = 3.007(1) mm/s at room temperature (Figure 3, Table 1). Given a

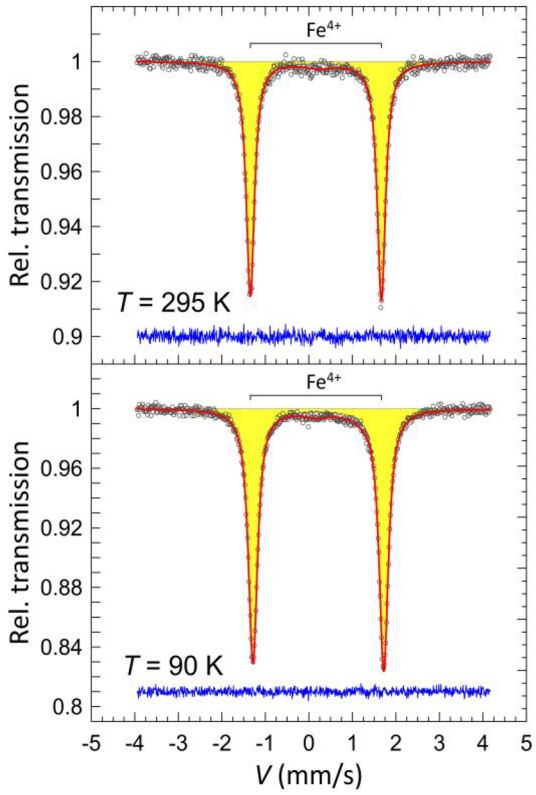

Figure 3. Mössbauer spectra of [Fe(tacn)(tfo)]Cl (**2**).

distorted octahedral coordination geometry of [Fe(tacn)(tfo)]Cl, the observed hyperfine parameters of Mössbauer spectra are consistent with the values expected for the triplet Fe(IV) complexes.[24,26−28,57,58] A large $|\Delta E_Q|$ indicates a relatively enhanced value of the electric field gradient presumably arising from deformation (e.g., stretching along the axis of the gradient) of the coordination octahedron around the Fe(IV) atom. No signs of decomposition were observed in the Mössbauer spectra of [Fe(tacn)(tfo)]Cl after 40 days at room temperature.

According to DFT calculations performed at the DFT-D3 level of theory with the BP86 functional, the triplet state was predicted to be most stable for complex $[Fe(tacn)(tfo)]^+$. Hypothetical singlet and pentet states were less stable by 9.0 and 20.7 kcal/mol, respectively. The optimized geometry of the triplet cation $[Fe(tacn)(tfo)]^+$ is in excellent agreement with the experimental X-ray data, while the high-spin structure shows significant deviations (see Supporting Information). Calculated Mössbauer isomer shifts and quadrupole splitting ΔE_Q calculated both for DFT-optimized (S = 1) and X-ray structures are in good agreement with experimental data (Table 2). Calculated δ and ΔE_Q values for

Table 2. Experimental and Calculated (DFT) Mössbauer Parameters of [Fe(tacn)(tfo)]Cl (2)

approach	S	T, K	δ (mm/s)	ΔE_Q (mm/s)	Γ (mm/s)
experiment		295	0.155(1)	|3.007(1)|	0.228(2)
experiment		90	0.218(1)	|3.007(1)|	0.256(1)
calculation[a,b]	1		0.19	−2.00	
calculation[a,c]	1		0.20	−2.21	
calculation[a,c]	0		0.16	−1.56	
calculation[a,c]	2		0.39	−1.51	

[a]RHO was calculated with the B3LYP DFT functional using the CP(PPP) basis set on Fe and the def2-TZVP basis set on other atoms. The electric field gradient was calculated using the TPSS DFT functional with the DKH-def2-QZVPP basis set on Fe and the def2-TZVP basis set on other atoms was used. Relativistic effects were taken into account by requesting a Douglas−Kroll−Hess second order scalar relativistic calculation. [b]Calculations were performed for the X-ray structure. [c]Calculations were performed for the DFT-optimized structure (DFT-D3 level of theory with BP86 functional was used for geometry optimization and calculations of thermochemistry).

low and high-spin structures substantially differ from the experiment (Table 2). According to a Mulliken population analysis of the triplet state structure, the spin density is almost fully localized on the iron atom (1.79 of 2 electrons, Figure 4a). These computational data provide strong evidence for the correct assignment of the ground state electron configuration close to d^4 for the iron atom.

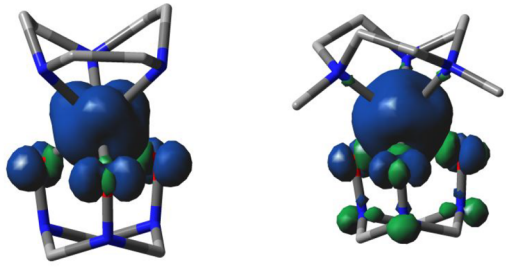

(a) [Fe(*tacn*)(*tfo*)]$^+$ (b) [Mn(*Me*$_3$*tacn*)(*tfo*)]$^+$

Figure 4. Calculated spin density in iron(IV)-tfo and manganese(IV)-tfo complexes **2** and **5**.

Similar DFT calculations of manganese complex $[Mn(Me_3tacn)(tfo)]^+$ revealed that the high-spin complex (S = 3/2) is more stable than the low-spin structure (S = 1/2) by 18.4 kcal/mol. The optimized geometrical parameters of the high-spin complex are very close to those derived from the X-ray analysis. The molecular orbital picture of this complex shows that three SOMOs are almost pure d_{z^2}, $d_{x^2-y^2}$, and d_{xy} Mn-derived orbitals (Figure 5). All three unpaired electrons are localized on a manganese atom according to Mulliken population analysis supporting the d^3 electronic configuration

https://doi.org/10.1021/acs.inorgchem.0c03362
Inorg. Chem. 2021, 60, 5523−5537

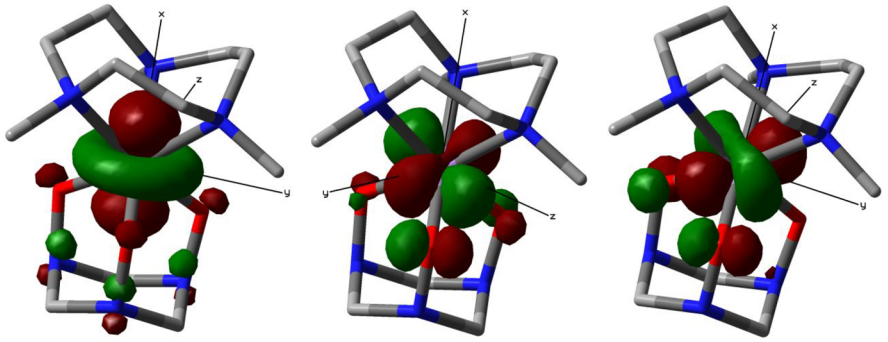

Figure 5. Calculated SOMO orbitals of $[Mn(Me_3tacn)(tfo)]^+$.

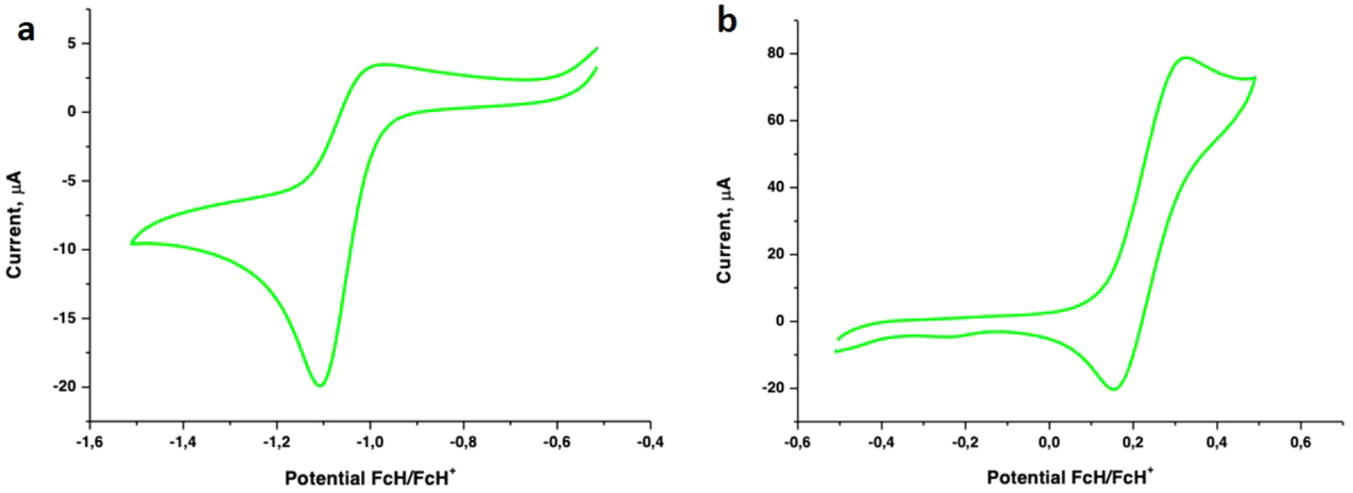

Figure 6. Electrochemical data for a 1 mM dimethylformamide solution of the iron complex [Fe(tacn)(tfo)]Cl (**2**) with 0.1 M $(n\text{-}(C_4H_9)_4N)PF_6$ as a supporting electrolyte: (a) cyclic voltammogram for the first reduction process, (b) cyclic voltammogram for the first oxidation process.

(Figure 4b). Interestingly, DFT calculations revealed that the order of d orbitals (d_{z^2} the lowest, then $d_{x^2-y^2}$ and d_{xy}) is different from typical octahedral splitting; the same splitting caused by the trigonal symmetry is characteristic of complexes with an encapsulated metal ion (clathrochelates[59]), such as iron(IV),[24] and often results in unusual magnetic properties, such as giant magnetic anisotropy[60] and single molecule magnet behavior.[61]

For nickel complex $[Ni(tacn)(tfo)]^+$, we were able to localize only one structure with d^6 configuration. This structure has the singlet (S = 0) ground state and is in good agreement with the X-ray data for complex **3**. Interestingly, two complexes having d^7 and d^8 configurations with large spin densities on N−O groups were also identified as local minima (see Supporting Information). The optimized geometry of both high-spin complexes showed significant distortion of the metalloadamantane unit, in which one M−O distance was elongated (2.37 Å for d^7, 3.50 Å for d^8) compared to the other two bonds (1.91 Å for d^7, 1.98 Å for d^8). According to Mulliken population analysis, the longer M−O distances are formed with nitroxide radical groups. However, these high-spin complexes were separated from the parent diamagnetic d^6 complex by 22.6 and 41.3 kcal/mol, respectively.

Electrochemical Properties. Redox properties for the complexes obtained were accessed by cyclic (CV) and differential pulse (DPV) voltammetries in a dimethylformamide/TBAP solution (Figure 6 and Figures S6−S8 in the Supporting Information). For the iron and nickel complexes **2** and **3**, one irreversible oxidation wave (with E_0 equal to 0.23 and 0.21 V referenced to the Fc/Fc^+ couple) and one irreversible reduction wave (at E_0 = −1.0 and −1.2 V) were detected by CV voltammetry; the manganese complex **4** features several irreversible reductions (Figure S8 in the Supporting Information). All the above waves show an almost irreversible behavior at a scan rate of 0.1 V s^{-1}; the increase in the scan rate leads to a quasi-reversible behavior in the case of the iron- and nickel-centered processes. The linear dependence of the peak current on the square root of the scan rate (Figures S6d, S7d in Supporting Information) suggests a diffusion-limited process. Note that the observed redox potentials are very close to those previously reported for a clathrochelate iron(IV) complex with a similar trigonal prismatic geometry.[24] Thus, ligand tfo^{3-} provides very efficient stabilization of the highly oxidized metal center.

The Nature of Stabilization of High-Valent Metals in Complexes with tfo Ligand. Geometrically, $[M(tacn)(tfo)]^+$ cations are somewhat similar to complexes of deprotonated all-*cis*-cyclohexanetriol and related ligands (in particular, 1,3,5-triamino-1,3,5-trideoxy-inositol *taci*).[62,63] However, these ligands do not form complexes with late D-metals in high oxidation states. Due to the presence of M−O−N motifs, $[M(tacn)(tfo)]^+$ complexes can be considered as analogs of metal hydroxamates, in particular hydroxamate

https://doi.org/10.1021/acs.inorgchem.0c03362
Inorg. Chem. 2021, 60, 5523−5537

sideophores.[64] Although anionic hydroxamate ligands can form M(IV) complexes, the latter are derived from early transition metals.[65−69] Therefore, tfo^{3-} provides some additional electronic stabilization for the high-valent metal center.[70] One could assume that tfo^{3-} is a noninnocent ligand, which is oxidized by the metal. Indeed, hydroxylamines are known to be redox-active, forming corresponding nitroxide radicals or oxoammonium cations upon oxidation. Characteristic examples are nitroxide species TEMPO, AZADO, PROXYL, PINO, etc.[71] From this viewpoint, three canonical structures A1, B1, and C1 could be proposed to describe the electronic structure of $[M(tacn)(tfo)]^+$ complexes (Figure 7). These structures differ in the formal

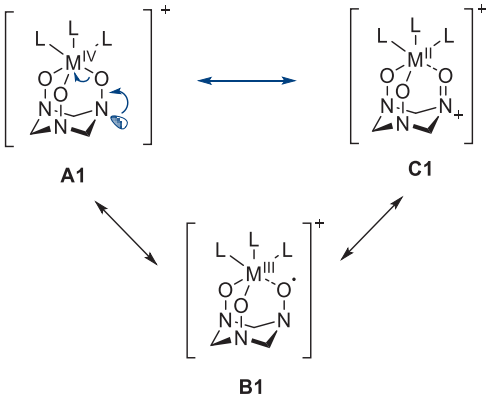

Figure 7. Canonical structures of metal(IV)-tfo complexes.

oxidation state of metal (from +2 to +4) and the oxidation level of the nitroxyl unit. Indeed, complexes of d-metals with hydroxylamines, nitroxide radicals, and oxoammonium cations having M−O−N, M−(*O−N), and M−(O=N$^+$) motifs, respectively, have been described in the literature.[72−79] In structures B1 and C1, the tfo ligand exhibits a mixed-valence state,[80,81] which may be apparent in the N−O bond stretching frequency in the IR spectra. The N−O bond stretching frequency strongly depends on the oxidation level of the nitroxide group (1000−900 cm^{-1} for hydroxylamines[44] and metal hydroxamates,[45,46] ca. 1350 cm^{-1} for nitroxide radicals[82] and ca. 1600 cm^{-1} for oxoammonium cations[83,84]). The position of ν(N−O) at 1015−963 cm^{-1} in $[M(tacn)(tfo)]^+$ complexes is indicative of a single nitrogen−oxygen bond, while the mixed valency of the ligand would result in a much higher frequency (intermediate between hydroxylamine and nitroxide radical or oxoammonium cation).

In our view, A1, B1, and C1 can be better viewed as resonance forms with the real structure of $[M(tacn)(tfo)]^+$ being likely a superposition of these canonical structures (this treatment makes the formal oxidation state of the metal meaningless). The relative contribution of these forms is different and may depend on the nature of the metal.

The geometrical parameters of octahedral Mn, Ni, and Fe complexes with nitroxide radicals substantially differ from those observed in $[M(tacn)(tfo)]^+$ complexes: M−O bond distances are much longer (>1.9 Å), and N−O bonds are considerably shorter (1.2−1.3 Å).[75,77,85,86] By these structural metrics as well as ν(N−O) frequencies, $[M(tacn)(tfo)]^+$ cations are closer to complexes with reduced TEMPO,[73,76] deprotonated hydroxylamines,[87] hydroxamic acids,[88] and *N*-oxides of tertial amines.[89,90] Thus, the nitroxide radical structure B1 does not seem to make a significant contribution to the structure of $[M(tacn)(tfo)]^+$ complexes. This is also confirmed by DFT calculations, which show very low spin density on the nitrogen and oxygen atoms (see Figure 4 and Supporting Information).

As for the canonic structure C1, the formation of a chelate would lead to a severe distortion of the sp^2 geometry of the nitrogen atom. For this reason, we believe that the contribution of the C1 form in the structure of $[M(tacn)(tfo)]^+$ is also small. On the other hand, canonical structure C1 clearly demonstrates the mechanism of additional stabilization of the d-metal ion by donation of the electron density from the *n*-orbital of nitrogen to metal d orbitals. The experimentally observed flattening of nitrogen atoms can be a consequence of these anomeric interactions. Hyperconjugation effects are known to be strong in organic adamantane derivatives due to their conformationally rigid structure and optimal geometry with staggered bonds.[43,91,92] Indeed, NBO analysis of $[Ni(tacn)(tfo)]^+$ revealed the presence of strong $n_N \rightarrow \sigma_{Ni-O}^*$ and interactions $n_N \rightarrow \sigma_{C-N}^*$ with energies of 4.8 and 6.6 kcal/mol.

Thus, the stabilization of high-valent metals in $[M(tacn)(tfo)]^+$ complexes can be explained by a strong σ-donor capacity of three anionic *N*-oxy groups of tfo^{3-} and additional donation of the electron density on the metal center from nitrogen atoms via hyperconjugation. These electronic effects are multiplied due to a tridentate nature of the tfo^{3-} ligand and the formation of a stable conformationally rigid adamantane structure.

Oxidation Reactivity and Catalytic Activity of Metal-tfo Complexes. Given the high oxidation state of the metal center, $[M(tacn)(tfo)]^+$ complexes are expected to exhibit oxidative properties. Indeed, iron(IV), manganese(IV), and nickel(IV) complexes are known to be reactive intermediates in biological and artificial catalytic oxidation processes.[26,27] However, $[M(tacn)(tfo)]^+Cl^-$ complexes were found to be indefinitely stable in the solid state and in solution (methanol and water). The UV−vis spectra monitoring showed no signs of decomposition of complexes **2**, **3**, and **5** in methanol and water at least within a week (c = 1 mM). More surprisingly, they were relatively stable in the acidic medium even in the presence of 165 equiv of trifluoroacetic acid. Complexes **2**, **3**, and **5** were resistant toward the action of oxidizable organic substrates such as hydroquinone, triphenylphoshine, and naphthalene (2 equiv of reducing agent, UV−vis control). However, with sodium ascorbate, dithionite, and sulfide, substantial changes in UV−vis spectra were observed (see Supporting Information). For example, the addition of 2 equiv of Na_2S to the nickel complex **3** resulted in an immediate disappearance of brown color. Surprisingly, after a few minutes under air, the initial brown color was restored. The recovery of the complex was confirmed by UV−vis monitoring shown in Figure 8. Similar behavior was observed for iron and manganese complexes **2** and **5**.

High-resolution mass spectra of the dark-red solution obtained by the reduction of [Fe(tacn)(tfo)]Cl (**2**) with sodium ascorbate contained a single cation $[Fe(tacn)(tfo)H]^+$, which corresponds to a protonated iron(III) complex. The same ion was observed in the reaction of $FeCl_3$ with tacn and $tfoH_3$ under an inert atmosphere (along with iron(IV) complex $[Fe(tacn)(tfo)]^+$). The ^{57}Fe Mössbauer spectra of both samples obtained by evaporation of these solutions contained a quadrupole doublet with an isomer shift of ca. δ 0.32 mm/s and a quadrupole splitting $|\Delta E_Q|$ of ca.

https://doi.org/10.1021/acs.inorgchem.0c03362
Inorg. Chem. 2021, 60, 5523−5537

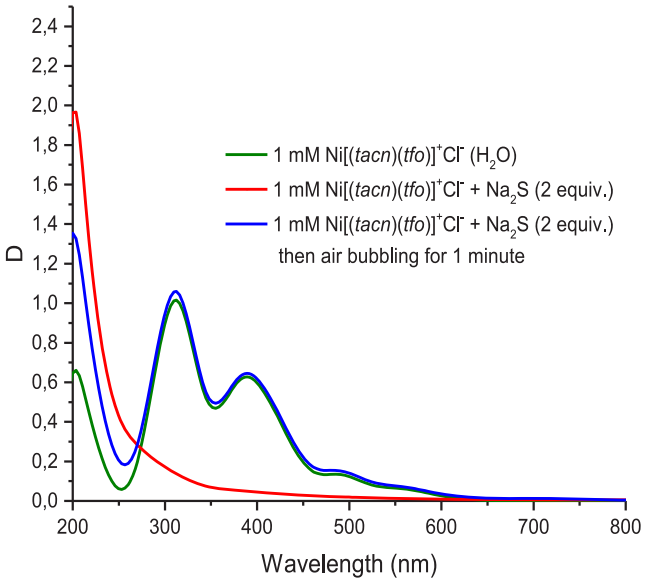

Figure 8. UV−vis monitoring of the reaction between complex **3** and Na_2S under an air atmosphere.

0.9 mm/s at room temperature. Compared to [Fe(tacn)(tfo)]Cl (**2**), the signal has a more positive isomer shift ($\Delta\delta$ = 0.17 mm/s) indicating a metal-centered reduction resulting in the formation of the high-spin (S = 5/2) iron complex. These Mössbauer parameters are in reasonable agreement with calculated values for electroneutral iron(III) complex [Fe(tacn)(tfo)] with S = 5/2. Upon exposure to air, this doublet disappears, and the formation of the [Fe(tacn)(tfo)]Cl complex is observed. However, our attempts to obtain single crystals for this complex failed. Further research will be performed to isolate and characterize metal(III)-tfo complexes.

The reversible character of reduction suggests that $[M(tacn)(tfo)]^+$ complexes may be catalytically active in the aerobic oxidation of sulfur compounds. Indeed, all three complexes (**2**, **3**, and **5**) exhibited catalytic activity in the aerobic oxidation of *p*-thiocresol to the corresponding disulfide with air under ambient conditions in methanol (Table 3). Iron complex **2** showed the highest catalytic activity with TON = 2000 and TOF = 83. With nickel complex **3**, 1 equiv of triethylamine was needed to achieve full conversion of thiol. The addition of TEMPO to the iron-catalyzed reaction did not result in a drop of the yield of disulfide. Moreover, in the presence of *N*-*tert*-butylmethanimine *N*-oxide, spin-trapping of thiyl radical was not observed by ESR. These experiments suggest that the oxidation of the thiol group proceeds via an ionic mechanism rather than a radical pathway.[93]

Table 3. Aerobic Oxidation of *p*-Thiocresol Catalyzed by Metal(IV)-tfo Complexes

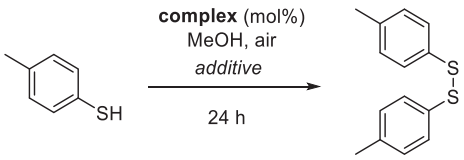

complex	mol %	additive	conversion	isolated yield of disulfide
[Fe(tacn)(tfo)]Cl (**2**)	0.1%		>99%	80%
[Ni(tacn)(tfo)]Cl (**3**)	0.5%	Et_3N	>99%	78%
[Mn(Me_3tacn)(tfo)]Cl (**5**)	0.5%	Et_3N	>99%	81%

Catalytic aerobic oxidation of thiols received some attention in recent years as it proves an efficient and wasteless method for the production of disulfides compared to conventional oxidizing reagents.[93−97] Although numerous aerobic methods have been developed based on noble and non-noble metal catalysts, they usually require high catalyst loadings,[93,97] elevated temperatures,[94−96] additives,[94] or photochemical activation.[97] To the best of our knowledge, iron complex [Fe(tacn)(tfo)]Cl (**2**) exhibits much higher activity in the oxidation of *p*-thiocresol compared to previously reported catalysts. We believe this can be a good starting point to develop a new generation of non-noble metal catalysts for aerobic oxidation of thiols and related sulfur compounds.

CONCLUSIONS

In conclusion, the structure of transition-metal-formaldoxime complexes (iron, nickel, and manganese) was revealed for the first time. According to the X-ray analysis, deprotonated formaldoxime cyclotrimer (tfo^{3-}) binds to the metal via three oxygen atoms forming an adamantane-like cage structure. The other three coordination vacancies are occupied by a macrocyclic triamine (tacn), which was used as a supporting ligand. The metal in [M(tacn)(tfo)]Cl has a formal +4 oxidation state, which is atypical for late transition metal complexes with organic ligands. The assignment of the ground state electronic configuration was confirmed by XPS, Mössbauer spectroscopy, NMR (Evans method), FT-IR spectroscopy, and DFT calculations. Interestingly, these indefinitely stable high-valent metal complexes are formed from the corresponding Fe(III), Ni(II), and Mn(II) salts by oxidation with air.

We believe that well-defined high-valent metal-formaldoxime complexes such as [M(tacn)(tfo)]Cl prepared in this work may find interesting applications in catalysis (aerobic oxidation reactions) and analytical chemistry (spectrophotometric determination of transition metals). As an illustration of this, we have shown that [M(tacn)(tfo)]Cl complexes exhibit high catalytic activity in the aerobic dehydrogenative dimerization of *p*-thiocresol under ambient conditions.

EXPERIMENTAL SECTION

General Methods and Instrumentation. All reactions were carried out in oven-dried (150 °C) glassware. CH_2Cl_2, $CHCl_3$, and Et_3N were distilled over CaH_2; THF was distilled over $LiAlH_4$. $Na_2[Fe(ON{=}CH_2)_6]$ was prepared according to a previously described protocol.[17] 1,4,7-Triazacyclononanetrihydrochloride (tacn •3HCl), *N*,*N*′,*N*″-trimethyl-1,4,7-triazacyclononane (Me_3tacn), 1,8-bis(dimethylamino)naphthalene (proton sponge), *p*-thiocresol, naphthalene, Ph_3P, hydroquinone, sodium ascorbate, and all inorganic reagents were commercial grade and used as received. NMR spectra were recorded at room temperature with residual solvent peaks as internal standards. Multiplicities are indicated by s (singlet), d (doublet), m (multiplet), and br (broad). Melting points were determined on a Kofler heating stage and were not corrected. HRMS experiments were performed on a mass-spectrometer with electrospray ionization and a time-of-flight (TOF) detector. Peaks in FT-IR spectra data are reported in cm^{-1} with the following relative

https://doi.org/10.1021/acs.inorgchem.0c03362
Inorg. Chem. 2021, 60, 5523−5537

intensities: s (strong), m (medium), w (weak), br (broad), and sh (shoulder). UV−vis spectra were recorded with the use of a Jasco V-770 spectrophotometer or SF2000 spectrophotometer for the solutions of the investigated compounds. Raman spectra were measured on Princeton Instruments SpectraPro with a CCD detector at laser wavelength λ = 671.7 nm, spot size ca. 2 μm, intervals 200−900 cm^{-1} and 800−1400 cm^{-1}, with 6 min of exposition on each interval. GC-MS was performed on a Chromatec 5000 with an Agilent DB-1MS column 122−0132.

Detailed information on the X-ray diffraction experiments, paramagnetic NMR, electrochemical measurements, XPS, ^{57}Fe Mössbauer absorption spectra, and DFT calculations is provided in the Supporting Information.

Synthesis of tfoH$_3$·HCl. *Method 1.* To a stirred formaldehyde solution (37 wt % in H_2O, 4.4 mL, 59 mmol) at 0 °C was added a hydroxylamine hydrochloride (4.0 g, 57 mmol). The mixture was stirred for 5 min at 0 °C, warmed up to room temperature, and stirred for an additional 2 h. The resulting solution was concentrated in a vacuum (80 Torr, 40 °C). Then, 5 mL of ethanol was added to the residue, and the mixture was left to stay in a refrigerator at 4 °C for 24 h. Then, another 10 mL of ethanol was added, and solid material was filtered off and was dried in a vacuum (0.2 Torr, 25 °C) to give 2.0 g (yield 61%) of tfoH$_3$·HCl as a white solid. ***Caution!*** *The product starts to decompose above 50 °C in a vacuum (0.1 Torr).* ^{1}H NMR spectrum of tfoH$_3$·HCl is in agreement with the literature data.[98] ^{1}H NMR (300 MHz, HSQC, D_2O, δ, ppm): 4.53 (s, 6 H, 3 CH_2). ^{13}C NMR (75 MHz, HSQC, D_2O, δ, ppm): 74.3 (CH_2). ESI-HRMS m/z [M-Cl]$^+$ calcd for $[C_3H_{10}N_3O_3]^+$: 136.0717. Found: 136.0718.

Method 2 (Used to Prepare ^{15}N-Labeled and Deuterated tfoH$_3$·HCl). To a stirred hydroxylamine hydrochloride solution (100 mg, 1.44 mmol) in H_2O (0.1 mL) was added a paraformaldehyde (43 mg, 1.44 mmol). The mixture was refluxed in a closed vial for 15 min until the formation of clear solution. The resulting solution was concentrated in a vacuum (80 Torr, 40 °C). Then, ethanol (150 uL) was added to the residue, and the mixture was left to stay in a refrigerator at 4 °C for 24 h. Then precipitate was separated from mother liquor, washed with ethanol (3 × 150 μL), and dried in a vacuum (0.2 Torr, 25 °C) to give 34 mg (yield 41%) of tfoH$_3$·HCl as a white solid. Mp. 108−112 °C. ***Caution!*** *The product starts to decompose above 50 °C in a vacuum (0.1 Torr).* ^{1}H NMR spectrum of tfoH$_3$·HCl is in agreement with the literature data.[98] ^{1}H NMR (300 MHz, D_2O, δ, ppm): 4.61 (s, 6 H, 3 CH_2). FT-IR (KBr): 3242 (s,br), 3034 (s,sh), 2835 (s,br), 2622 (s), 2523 (m), 2419 (w), 1541 (s), 1405 (s,br), 1348 (m), 1307 (w), 1253 (w), 1203 (s), 1178 (s), 1131 (s), 1039 (s), 973 (s), 947 (s), 889 (s), 796 (s), 709 (m), 622 (br), 557 (s), 503 (m), 431 (s). Anal. Calcd for $C_3H_{10}ClN_3O_3$: C, 21.00; H, 5.87; N, 24.49. Found: C, 21.16; H, 5.78; N, 23.86. Single crystals of tfoH$_3$·HCl, suitable for X-ray diffraction, were obtained by recrystallization from hot ethanolic solution. Using ^{15}N-hydroxylamine hydrochloride or D_2-paraformaldehyde, ^{15}N-labeled and deuterated samples of tfoH$_3$·HCl were prepared.

Fe(ON=CHNO)$_2$*py*$_2$ (1). To a solution of anhydrous $FeCl_3$ (150 mg, 0.93 mmol) in methanol (5 mL) were consequently added tfoH$_3$·HCl (159 mg, 0.93 mmol) and pyridine (0.63 mL, 7.8 mmol). The purple-brown solution was stirred at room temperature overnight under air. The resulting dark-olive solution was concentrated under reduced pressure. The residue was dried in a vacuum to remove the unreacted pyridine and then dissolved in water (20 mL). The aqueous layer was washed with a mixture of EtOAc-Et_2O until the organic layer became colorless. Then, $CHCl_3$ (20 mL) was added to the aqueous layer and the mixture was stirred overnight with access to air. The resulting deep-blue chloroform layer was separated and concentrated in a vacuum to give 7 mg of dark blue crystals of complex **1** (yield: 2%). Mp. above 280 °C. FT-IR (KBr): 3480 (br), 3074 (w), 2922 (w), 2851 (w), 1605 (m), 1487 (w), 1449 (s), 1407 (s), 1385 (s), 1373 (s), 1357 (s), 1238 (m), 1219 (m), 1096 (m), 1066 (m), 1030 (s), 876 (w), 830 (m), 799 (w), 763 (m), 695 (m), 643 (w), 606 (w). UV−vis spectrum: (CH_2Cl_2, c = 2.3 × 10^{-3} M) peaks λ nm: 600 (max. extinction coefficient ε_{max} = 0.8 × 10^3). ESI-HRMS m/z [M + H]$^+$ calcd for $[C_{12}H_{13}FeN_6O_4]^+$: 361.0342. Found: 361.0339.

[Fe(tacn)(tfo)]Cl (2). To a mixture of tfoH$_3$·HCl (34 mg, 0.2 mmol), tacn·3HCl (48 mg, 0.20 mmol), anhydrous $FeCl_3$ (32 mg, 0.20 mmol), and proton sponge (428 mg, 2.0 mmol) was added 5 mL of methanol. The reaction mixture was stirred for 1 h at room temperature under air and then kept for an additional 24 h with a closed cap. The precipitate was centrifuged off, and a clear solution containing complex **2** was concentrated in a vacuum. The residue was dried at 0.1 Torr for 30 min, and a mixture of Et_2O (10 mL) and CH_2Cl_2 (30 mL) was added to the crude product. The mixture was left to stay in a refrigerator at 4 °C for 4 days. Then precipitate was separated from the mother liquor and dried at 0.1 Torr for 30 min. The residue was placed in a centrifuge cup and centrifuged with CH_2Cl_2 (3 × 10 mL) and THF (2 × 10 mL). The residual solid was dissolved in 3 mL of methanol (dark maroon solution) and centrifuged. Clear solution was separated from a small amount of undissolved material and concentrated in a vacuum. This operation was repeated twice. Solid material was dried in a vacuum at 0.1 Torr to give 31 mg (yield 42%) of **2** as a black solid. Mp. above 280 °C. FT-IR (KBr): 3449 (br), 3240 (s), 3053 (s), 2978 (s), 2924 (m), 2883 (s), 2828 (w), 1631 (br), 1485 (w), 1450 (s), 1419 (m), 1360 (m), 1329 (w), 1261 (m), 1229 (w), 1167 (m), 1101 (s), 1042 (s), 972 (s), 929 (s), 874 (m), 830 (m), 779 (s), 746 (s), 632 (s), 604 (m), 530 (s), 460 (s), 431 (m). UV−vis spectrum (MeOH, c = 6.4 × 10^{-6} M), λ nm: 273 (max. extinction coefficient ε_{max} = 5.4 × 10^4), 345 (ε_{max} = 2.8 × 10^4), 492 (ε_{max} = 1.9 × 10^4), 578 (ε_{max} = 7.7 × 10^3). Raman spectrum: 217 (intensity: 340, Fe−O),[99] 289 (intens.: 161), 362 (intens.: 190), 387 (intens.: 202), 429 (intens.: 209), 462 (intens.: 120), 500 (intens.: 508, ν_sFe−O and Fe−N),[99] 524 (intens.: 792), 538 (intens.: 358), 632 (intens.: 227), 748 (intens.: 105), 976 (intens.: 148), 1250 (intens.: 2354, twisting CH_2 from tfo and tacn),[99] 1357 (intens.: 115), 1424 (intens.: 5818, scissoring CH_2 from tfo and tacn).[99−101] ESI-HRMS m/z [M-Cl]$^+$ calcd for $[C_9H_{21}FeN_6O_3]^+$: 317.1019. Found: 317.1021. Anal. Calcd for $C_9H_{21}ClFeN_6O_3$·0.5CH_3OH: C, 30.95; H, 6.29; N, 22.80. Found: C, 31.54; H, 5.95; N, 22.82. For synthesis and characterization of isotope-labeled complexes **2**, see Supporting Information.

[Ni(tacn)(tfo)]Cl·MeOH (3). To a mixture of tfoH$_3$·HCl (34 mg, 0.20 mmol), tacn·3HCl (48 mg, 0.20 mmol), anhydrous $NiCl_2$ (26 mg, 0.20 mmol), and proton sponge (428 mg, 2.0 mmol) was added 5 mL of methanol. The reaction mixture was stirred for 1 h at room temperature under air and then for an additional 24 h with a closed cap. The precipitate was centrifuged off, and clear solution was concentrated in a vacuum. The residue was dried at 0.1 Torr for 30 min, and a mixture of Et_2O (10 mL) and CH_2Cl_2 (30 mL) was added to the crude product. The mixture was left to stay in a refrigerator at 4 °C for 2 days. Then, the precipitate was separated from the mother liquor (off-white solid was not collected) and dried in a vacuum at 0.1 Torr for 30 min. The residue was placed in a centrifuge cup and centrifuged with CH_2Cl_2 (5 × 8 mL) and THF (2 × 10 mL). Solid residue was dissolved in 3 mL of methanol (dark maroon solution) and concentrated in a vacuum. The resulting crude material was dissolved in 1 mL of methanol; clear solution was separated from a small amount of off-white solid and evaporated again. This operation was repeated with 0.4 mL of methanol and then with 0.2 mL of methanol (until clear solution is formed upon dissolution in methanol). The residue was dried in a vacuum at 0.1 Torr to give 22 mg (yield 28%) of **3** as a black solid. Mp. above 280 °C. ^{1}H NMR (300 MHz, HSQC, COSY, D_2O, δ, ppm, J/Hz): 2.73 (d, J = 11.6 Hz, 3 H, CH_2), 3.04 (m, 6 H, CH_2−CH_2), 3.30 (m, 6 H, CH_2−CH_2), 3.38 (br. s, CH_3OH), 3.97 (br, 3 H, NH), 5.13 (d, J = 11.6 Hz, 3 H, CH_2). ^{13}C NMR (75 MHz, HSQC, D_2O, δ, ppm): 45.9 (CH_2-CH_2), 86.0 (CH_2). FT-IR (KBr): 3434 (br), 3255 (s, br), 3195 (s, br), 2944 (m), 2893 (br), 1631 (m, br), 1454 (m), 1428 (m), 1366 (m), 1327 (m), 1278 (w), 1220 (m), 1103 (s), 1049 (s), 1015 (s), 955 (m), 925 (s), 874 (m), 831 (m), 762 (m), 625 (s), 592 (m), 539 (w), 508 (m), 445 (s), 419

https://doi.org/10.1021/acs.inorgchem.0c03362
Inorg. Chem. 2021, 60, 5523−5537

(w). UV−vis spectrum (MeOH, c = 8.5 × 10^{-6} M), λ nm: 211 (max. extinction coefficient ε_{max} = 2.5 × 10^4), 256 (ε_{max} = 1.7 × 10^4), 303 (ε_{max} = 4.8 × 10^4), 367 (ε_{max} = 2.8 × 10^4). ESI-HRMS m/z [M-Cl]$^+$ calcd for $[C_9H_{21}N_6NiO_3]^+$: 319.1023. Found: 319.1016. Anal. Calcd for $C_9H_{21}ClNiN_6O_3{\cdot}CH_3OH$: C, 31.00; H, 6.50; N, 21.69. Found: C, 30.74; H, 6.13; N, 21.29. For synthesis and characterization of isotope-labeled complexes **3** see Supporting Information.

[Mn(tacn)(tfo)]Cl (4). To a mixture of $tfoH_3{\cdot}HCl$ (64 mg, 0.38 mmol), tacn·3HCl (90 mg, 0.38 mmol) and $Mn(OAc)_3{\cdot}2H_2O$ (102 mg, 0.38 mmol) was added 3 mL of methanol. After 15 min of stirring, Et_3N (0.53 mL, 3.8 mmol) was added. The reaction mixture was stirred for 1 h at room temperature under air and then for an additional 24 h with a closed cap. The resulting mixture was concentrated at 80 Torr. The residue was triturated with a $CHCl_3$-Et_2O mixture (5 mL: 5 mL). The solid material was separated from the mother liquor and dried in a vacuum for 8 h at 100 °C (off-white solid was not collected). The resulting crude material was triturated with 5 mL of $CHCl_3$ and dried at 0.1 Torr to give 47 mg (yield 35%) of **4** as a black solid. Mp. above 250 °C. ESI-HRMS m/z [M-Cl]$^+$ calcd for $[C_9H_{21}MnN_6O_3]^+$: 316.1050. Found: 316.1047. Anal. Calcd for $C_9H_{21}ClMnN_6O_3$: C, 30.74; H, 6.02; N, 23.90. Found: C, 30.74; H, 6.07; N, 23.89.

Synthesis of [Mn(tacn)(tfo)]Cl (4) from $MnCl_2$. To a mixture of $tfoH_3{\cdot}HCl$ (34 mg, 0.20 mmol), anhydrous $MnCl_2$ (25 mg, 0.20 mmol), tacn·3HCl (48 mg, 0.20 mmol), and proton sponge (428 mg, 2.0 mmol) was added 5 mL of methanol. The reaction mixture was stirred for 1 h at room temperature under air and then for an additional 48 h with a closed cap. The precipitate was centrifuged off, and the solution was concentrated in a vacuum. The residue was dried at 0.1 Torr for 1 h, and a mixture of Et_2O (20 mL) and CH_2Cl_2 (30 mL) was added to the crude product. The mixture was kept at 4 °C for 3 days. Then, the precipitate was separated from the mother liquor and dried at 0.1 Torr for 30 min (off-white solid was not collected). The resulting brown solid was placed in a centrifuge cup and centrifuged with CH_2Cl_2 (3 × 10 mL). The residual solid was dissolved in 3 mL of methanol (dark maroon solution) and centrifuged. Clear solution was separated from a small amount of undissolved material and concentrated in a vacuum. To the residual solid was added 1 mL of methanol; the clear solution was separated from insoluble solid and concentrated in a vacuum. This operation was repeated with 0.4 mL of methanol (until clear solution is formed upon dissolution in methanol). The residue was dried at 0.1 Torr to give 20 mg (yield 26%) of complex **4** as a black solid. This procedure was used to prepare isotope-labeled complexes **4** (for details, see Supporting Information).

[Mn(*Me*$_3$tacn)(tfo)]Cl·MeOH (5). To a mixture of $tfoH_3{\cdot}HCl$ (34 mg, 0.20 mmol), anhydrous $MnCl_2$ (25 mg, 0.20 mmol), and proton sponge (300 mg, 1.40 mmol) were added 5 mL of methanol and Me_3tacn (0.39 mL, 0.20 mmol). The reaction mixture was stirred for 1 h at room temperature under air and then for an additional 24 h with a closed cap. The precipitate was centrifuged off, and the solution was concentrated in a vacuum. The residue was dried at 0.1 Torr for 1 h, and a mixture of Et_2O (20 mL) and CH_2Cl_2 (30 mL) was added to the crude product. The mixture was left to stay in a refrigerator at 4 °C for 4 days. Then, precipitate was separated from the mother liquor and dried at 0.1 Torr for 30 min (off-white solid was not collected). The resulting brown solid was placed in a centrifuge cup and centrifuged with a CH_2Cl_2-Et_2O mixture (5 mL: 5 mL) and with a CH_2Cl_2-Et_2O mixture (4.5 mL: 2.5 mL). To the residual solid was added 3 mL of methanol; the clear solution was separated from insoluble crystals and concentrated in a vacuum. The last operation was repeated with 1 mL of methanol and then with 0.4 mL of methanol (until clear solution is formed upon dissolution in methanol). The residue was dried at 0.1 Torr to give 14 mg (yield 15%) of **5** as a black solid. Mp. above 280 °C. FT-IR (KBr): 3382 (br), 2994 (m), 2934 (m), 2849 (m), 2624 (w;br), 1697 (w), 1658 (w) 1599 (w), 1501 (m), 1462 (s), 1415 (m), 1382 (m), 1345 (w), 1290 (s), 1252 (w), 1202 (w), 1160 (s), 1121 (w), 1058 (s), 1003 (s), 970 (s), 931 (s), 901 (m), 868 (w), 784 (s), 738 (s), 661 (w), 619 (s), 591 (m), 509 (s), 451 (s). UV−vis spectrum (MeOH, c = 5.8 × 10^{-6} M), λ nm: 211 (max. extinction coefficient ε_{max} = 2.7 × 10^4), 252 (ε_{max} = 3.7 × 10^4), 297 (ε_{max} = 3.6 × 10^4), 451 (ε_{max} = 2.6 × 10^4), 542 (ε_{max} = 6.8 × 10^3). ESI-HRMS m/z [M-Cl]$^+$ calcd for $[C_{12}H_{27}MnN_6O_3]^+$: 358.1520. Found: 358.1525. Anal. calcd for $C_{12}H_{27}ClMnN_6O_3{\cdot}2CH_3OH{\cdot}H_2O$: C, 35.34; H, 7.84; N, 17.66. Found: C, 34.89; H, 7.47; N, 17.42.

Aerobic Oxidation of *p*-Thiocresol Catalyzed by Fe[(tacn)(tfo)]Cl. A solution of *p*-thiocresol (25 mg, 0.2 mmol, 1000 equiv) in methanol (250 μL) was added to a 1 mM solution of Fe[(tacn)(tfo)]$^+$Cl$^-$ in methanol (200 μL, 0.0002 mmol, 1 equiv). The mixture was stirred in a closed vessel equipped with a magnetic stirrer and an air-filled balloon for 24 h. The resulting solution was concentrated under reduced pressure. Hexane (2 mL) and water (1 mL) were added to the residue. The organic phase was collected, and the aqueous layer was washed with hexane (2 × 2 mL). The combined organic phase was dried over anhydrous sodium sulfate, concentrated under reduced pressure, and dried to a constant weight to give 19.7 mg (80%) of *p*-tolyl disulfide as a white solid. Mp. 46 °C (lit.[102] 43−46 °C). GC-MS: r.t. 10.1 min; m/z = 246 ([M]$^{+}$*). ^{1}H NMR spectrum of *p*-tolyl disulfide is in agreement with the literature data.[102] ^{1}H NMR (300 MHz, $CDCl_3$, δ, ppm): 2.32 (s, 6 H), 7.09 (m, 4 H), 7.37 (m, 4 H).

Safety Note! *Formaldehyde is highly toxic upon inhalation/ingestion and corrosive upon skin and eye contact. All operations must be conducted in a fume hood with suitable protection and precautions taken.*

■ ASSOCIATED CONTENT

Supporting Information

The Supporting Information is available free of charge at https://pubs.acs.org/doi/10.1021/acs.inorgchem.0c03362.

Detailed experimental procedures, crystallographic data and characterization data for all compounds, copies of XPS, Mössbauer, FT-IR, UV−vis, NMR, Raman and mass spectra, details of DFT calculations, and electrochemical studies (PDF)

Animated N−O stretching frequency of compound **2** (AVI)

Animated N−O stretching frequency of compound **3** (AVI)

Animated N−O stretching frequency of compound **4** (AVI)

Accession Codes

CCDC 2035754−2035757 and 2061527 contain the supplementary crystallographic data for this paper. These data can be obtained free of charge via www.ccdc.cam.ac.uk/data_request/cif, or by emailing data_request@ccdc.cam.ac.uk, or by contacting The Cambridge Crystallographic Data Centre, 12 Union Road, Cambridge CB2 1EZ, UK; fax: +44 1223 336033.

■ AUTHOR INFORMATION

Corresponding Author

Alexey Yu. Sukhorukov − *N. D. Zelinsky Institute of Organic Chemistry, Russian Academy of Sciences, Moscow, Russia 119991; Plekhanov Russian University of Economics, Moscow, Russia 117997;* orcid.org/0000-0003-4413-9453; Email: sukhorukov@ioc.ac.ru

Authors

Ivan S. Golovanov − *N. D. Zelinsky Institute of Organic Chemistry, Russian Academy of Sciences, Moscow, Russia 119991;* orcid.org/0000-0001-7219-2409

Roman S. Malykhin − *N. D. Zelinsky Institute of Organic Chemistry, Russian Academy of Sciences, Moscow, Russia 119991*

Vladislav K. Lesnikov − *N. D. Zelinsky Institute of Organic Chemistry, Russian Academy of Sciences, Moscow, Russia 119991*

Yulia V. Nelyubina − *A. N. Nesmeyanov Institute of Organoelement Compounds, Russian Academy of Sciences, Moscow, Russia 119991*

Valentin V. Novikov − *A. N. Nesmeyanov Institute of Organoelement Compounds, Russian Academy of Sciences, Moscow, Russia 119991;* orcid.org/0000-0002-0225-0594

Kirill V. Frolov − *Shubnikov Institute of Crystallography of FSRC "Crystallography and Photonics," Russian Academy of Sciences, Moscow, Russia 119991*

Andrey I. Stadnichenko − *Boreskov Institute of Catalysis, Siberian Branch of Russian Academy of Sciences, Novosibirsk, Russia 630090*

Evgeny V. Tretyakov − *N. D. Zelinsky Institute of Organic Chemistry, Russian Academy of Sciences, Moscow, Russia 119991;* orcid.org/0000-0003-1540-7033

Sema L. Ioffe − *N. D. Zelinsky Institute of Organic Chemistry, Russian Academy of Sciences, Moscow, Russia 119991*

Complete contact information is available at: https://pubs.acs.org/10.1021/acs.inorgchem.0c03362

Author Contributions

The manuscript was written through contributions of all authors. All authors have given approval to the final version of the manuscript.

Notes

The authors declare no competing financial interest.

■ ACKNOWLEDGMENTS

The reported study was funded by the Russian Foundation for Basic Research (project # 20-33-70188). X-ray diffraction data were collected using the equipment of the Center for Molecular Composition Studies of INEOS RAS with financial support from the Ministry of Science and Higher Education of the Russian Federation. Mossbauer and Raman spectroscopy studies were supported by the Russian Ministry of Science and Higher Education within the State assignment of the FSRC "Crystallography and Photonics" of RAS. The authors acknowledge Dr. Ivan A. Troyan (Shubnikov Institute of Crystallography of FSRC "Crystallography and Photonics" of RAS) for the Raman spectroscopy measurements and Vladislav M. Korshunov (P. N. Lebedev Physical Institute of RAS) for the UV−vis spectroscopy measurements.

■ REFERENCES

(1) Dunstan, W. R.; Bossi, A. L. XXXV.—The preparation and properties of formaldoxime. *J. Chem. Soc., Trans.* **1898**, *73*, 353.

(2) Hofmann, K. A.; Ehrhardt, U. Innerkomplexe Metallsalze der Oxalsäure-Derivate und des Triform-oxims. *Ber. Dtsch. Chem. Ges.* **1913**, *46*, 1457.

(3) Marczenko, Z. Dosage spectrophotometrique de differents metaux (Mn, Ce, V, Ni, Fe) au moyen de la formaldoxime. *Anal. Chim. Acta* **1964**, *31*, 224.

(4) Bradfield, E. G. An improved formaldoxime method for the determination of manganese in plant material. *Analyst* **1957**, *82*, 254.

(5) Goto, K.; Komatsu, T.; Furukawa, T. Rapid colorimetric determination of manganese in waters containing iron: A modification of the formaldoxime method. *Anal. Chim. Acta* **1962**, *27*, 331.

(6) Youngvises, N.; Suwannasaroj, K.; Jakmunee, J.; AlSuhaimi, A. Multi-reverse flow injection analysis integrated with multi-optical sensor for simultaneous determination of Mn(II), Fe(II), Cu(II) and Fe(III) in natural waters. *Talanta* **2017**, *166*, 369.

(7) Grebel, J. E.; Charbonnet, J. A.; Sedlak, D. L. Oxidation of organic contaminants by manganese oxide geomedia for passive urban stormwater treatment systems. *Water Res.* **2016**, *88*, 481.

(8) Kaewwonglom, N.; Jakmunee, J. Sequential injection system with multi-parameter analysis capability for water quality measurement. *Talanta* **2015**, *144*, 755.

(9) Zhu, M.; Ginder-Vogel, M.; Parikh, S. J.; Feng, X.-H.; Sparks, D. L. Cation Effects on the Layer Structure of Biogenic Mn-Oxides. *Environ. Sci. Technol.* **2010**, *44*, 4465.

(10) Koeber, K.; Kottelwesch, H.; Schneider, D. In *Mn Manganese*; Demmer, H., Kottelwesch, H., Schleitzer-Rust, E., Eds.; Springer-Verlag: Berlin, 1987; p 232.

(11) Henriksen, A. An automatic, modified formaldoxime method for determining low concentrations of manganese in water containing iron. *Analyst* **1966**, *91*, 647.

(12) Derie, R. Formaldehyde oxime leaching of metals from deep-sea manganese nodules and other ores. *Nature* **1986**, *324*, 660.

(13) Bartušek, M.; Okáč, A. Über die Komplexsalze des Formaldoxims II. Isolierung von Nickel-, Mangan-und Kobaltkomplexen. *Collect. Czech. Chem. Commun.* **1961**, *26*, 883.

(14) Bartušek, M.; Okáč, A. Über die Komplexsalze des Formaldoxims. *Collect. Czech. Chem. Commun.* **1961**, *26*, 52.

(15) Bartušek, M.; Okáč, A. Über komplexsalze des formaldoxims III. Komplexverbindungen des nickels, mangans und kobalts. *Collect. Czech. Chem. Commun.* **1961**, *26*, 2174.

(16) Bečka, J.; Jokl, J. Papierelektrophorese von Komplexverbindungen des Formaldoxims mit Mangan, Nickel, Eisen und Vanadin. *Collect. Czech. Chem. Commun.* **1971**, *36*, 2467.

(17) Andersen, F. A.; Jensen, K. A. Infrared spectra of transition metal coordination compounds with the formaldoximate ion. *J. Mol. Struct.* **1980**, *60*, 165.

(18) Andersen, F. A.; Jensen, K. A. Infrared spectroscopic study of some transition metal compounds with coordinated formaldoximate ion. *J. Mol. Struct.* **1982**, *79*, 357.

(19) Andersen, F. A.; Jensen, K. A. The configuration of transition metal coordination compounds containing the anion of hexahydro-1,3,5-triazine-1,3,5-triol. *J. Mol. Struct.* **1986**, *141*, 441.

(20) Golovanov, I. S.; Sukhorukov, A. Y.; Nelyubina, Y. V.; Khomutova, Y. A.; Ioffe, S. L.; Tartakovsky, V. A. Synthesis of B,O,N-Doped Adamantanes and Diamantanes by Condensation of Oximes with Boronic Acids. *J. Org. Chem.* **2015**, *80*, 6728.

(21) Gouzerh, P.; Jeannin, Y.; Rocchiccioli-Deltcheff, C.; Valentini, F. Synthesis, properties and structure of tris(ethylnitrosolato) complexes of manganese, iron, and cobalt. *J. Coord. Chem.* **1979**, *9*, 221.

(22) With cobalt, cation $[Co(tacn)(tfo)]^+$ was observed in ESI-HRMS; however, attempts to crystallize this complex failed.

(23) With trispyrazolylborate, HRMS revealed the formation of the $[Mn(trispyrazolylborate)_2]^+$ complex.

(24) Tomyn, S.; Shylin, S. I.; Bykov, D.; Ksenofontov, V.; Gumienna-Kontecka, E.; Bon, V.; Fritsky, I. O. Indefinitely stable iron(IV) cage complexes formed in water by air oxidation. *Nat. Commun.* **2017**, *8*, 14099.

(25) Malischewski, M.; Adelhardt, M.; Sutter, J.; Meyer, K.; Seppelt, K. Isolation and structural and electronic characterization of salts of the decamethylferrocene dication. *Science* **2016**, *353*, 678.

(26) McDonald, A. R.; Que, L. High-valent nonheme iron-oxo complexes: Synthesis, structure, and spectroscopy. *Coord. Chem. Rev.* **2013**, *257*, 414.

(27) Hohenberger, J.; Ray, K.; Meyer, K. The biology and chemistry of high-valent iron-oxo and iron-nitrido complexes. *Nat. Commun.* **2012**, *3*, 720.
(28) Chanda, A.; Shan, X.; Chakrabarti, M.; Ellis, W. C.; Popescu, D. L.; Tiago de Oliveira, F.; Wang, D.; Que, L.; Collins, T. J.; Münck, E.; Bominaar, E. L. (TAML)FeIV═O Complex in Aqueous Solution: Synthesis and Spectroscopic and Computational Characterization. *Inorg. Chem.* **2008**, *47*, 3669.
(29) Chanda, A.; Popescu, D.-L.; de Oliveira, F. T.; Bominaar, E. L.; Ryabov, A. D.; Münck, E.; Collins, T. J. High-valent iron complexes with tetraamido macrocyclic ligands: Structures, Mössbauer spectroscopy, and DFT calculations. *J. Inorg. Biochem.* **2006**, *100*, 606.
(30) Ghosh, A.; Tiago de Oliveira, F.; Yano, T.; Nishioka, T.; Beach, E. S.; Kinoshita, I.; Münck, E.; Ryabov, A. D.; Horwitz, C. P.; Collins, T. J. Catalytically Active μ-Oxodiiron(IV) Oxidants from Iron(III) and Dioxygen. *J. Am. Chem. Soc.* **2005**, *127*, 2505.
(31) Shylin, S. I.; Pavliuk, M. V.; D'Amario, L.; Mamedov, F.; Sá, J.; Berggren, G.; Fritsky, I. O. Efficient visible light-driven water oxidation catalysed by an iron(iv) clathrochelate complex. *Chem. Commun.* **2019**, *55*, 3335.
(32) Meucci, E. A.; Ariafard, A.; Canty, A. J.; Kampf, J. W.; Sanford, M. S. Aryl-Fluoride Bond-Forming Reductive Elimination from Nickel(IV) Centers. *J. Am. Chem. Soc.* **2019**, *141*, 13261.
(33) Padamati, S. K.; Angelone, D.; Draksharapu, A.; Primi, G.; Martin, D. J.; Tromp, M.; Swart, M.; Browne, W. R. Transient Formation and Reactivity of a High-Valent Nickel(IV) Oxido Complex. *J. Am. Chem. Soc.* **2017**, *139*, 8718.
(34) Martinez, G. E.; Ocampo, C.; Park, Y. J.; Fout, A. R. Accessing Pincer Bis(carbene) Ni(IV) Complexes from Ni(II) via Halogen and Halogen Surrogates. *J. Am. Chem. Soc.* **2016**, *138*, 4290.
(35) Camasso, N. M.; Sanford, M. S. Design, synthesis, and carbon-heteroatom coupling reactions of organometallic nickel(IV) complexes. *Science* **2015**, *347*, 1218.
(36) Carnes, M.; Buccella, D.; Chen, J. Y.-C.; Ramirez, A. P.; Turro, N. J.; Nuckolls, C.; Steigerwald, M. A Stable Tetraalkyl Complex of Nickel(IV). *Angew. Chem., Int. Ed.* **2009**, *48*, 290.
(37) Singh, A. B. Spectroscopic and Electrochemical Studies of Nickel(III) and Nickel(IV) Complexes derived From Oximato Ligands. *Synth. React. Inorg. Met.-Org. Chem.* **1986**, *16*, 433.
(38) Baucom, E. I.; Drago, R. S. Nickel(II) and nickel(IV) complexes of 2,6-diacetylpyridine dioxime. *J. Am. Chem. Soc.* **1971**, *93*, 6469.
(39) Alvarez, S. Relationships between Temperature, Magnetic Moment, and Continuous Symmetry Measures in Spin Crossover Complexes. *J. Am. Chem. Soc.* **2003**, *125*, 6795.
(40) Semakin, A. N.; Sukhorukov, A. Y.; Lesiv, A. V.; Ioffe, S. L.; Lyssenko, K. A.; Nelyubina, Y. V.; Tartakovsky, V. A. Unusual Intramolecular Cyclization of Tris(β-oximinoalkyl)amines. The First Synthesis of 1,4,6,10-Tetraazaadamantanes. *Org. Lett.* **2009**, *11*, 4072.
(41) Semakin, A. N.; Nelyubina, Y. V.; Ioffe, S. L.; Sukhorukov, A. Y. 2,4,9-Triazaadamantanes with "Clickable" Groups: Synthesis, Structure and Applications as Tripodal Platforms. *Eur. J. Org. Chem.* **2020**, *2020*, 6723.
(42) Jerslev, B.; Brehm, L.; Gabrielsen, M. V. The Crystal Structure and the Conformation of 1,3,5-Triacetoxyhexahydro-1,3,5-triazine. *Acta Chem. Scand.* **1977**, *31*, 875.
(43) Semakin, A. N.; Sukhorukov, A. Y.; Nelyubina, Y. V.; Khomutova, Y. A.; Ioffe, S. L.; Tartakovsky, V. A. Urotropine Isomer (1,4,6,10-Tetraazaadamantane): Synthesis, Structure, and Chemistry. *J. Org. Chem.* **2014**, *79*, 6079.
(44) Nightingale, R. E.; Wagner, E. L. The Vibrational Spectra and Structure of Solid Hydroxylamine and Deutero-Hydroxylamine. *J. Chem. Phys.* **1954**, *22*, 203.
(45) Edwards, D. C.; Nielsen, S. B.; Jarzęcki, A. A.; Spiro, T. G.; Myneni, S. C. B. Experimental and theoretical vibrational spectroscopy studies of acetohydroxamic acid and desferrioxamine B in aqueous solution: Effects of pH and iron complexation. *Geochim. Cosmochim. Acta* **2005**, *69*, 3237.
(46) Bhatt, K.; Agrawal, Y. K. Hydroxamic Acids and Their Metal Complexes: Preparation, Properties, and Infrared Spectra. *Synth. React. Inorg. Met.-Org. Chem.* **1972**, *2*, 175.
(47) Yang, J.; Bremer, P. J.; Lamont, I. L.; McQuillan, A. J. Infrared Spectroscopic Studies of Siderophore-Related Hydroxamic Acid Ligands Adsorbed on Titanium Dioxide. *Langmuir* **2006**, *22*, 10109.
(48) Evans, D. 400. The determination of the paramagnetic susceptibility of substances in solution by nuclear magnetic resonance. *J. Chem. Soc.* **1959**, 2003.
(49) NIST X-ray Photoelectron Spectroscopy Database, NIST Standard Reference Database Number 20, National Institute of Standards and Technology: Gaithersburg, MD, 2000, 20899.
(50) Zhou, A.-J.; Liu, J.-L.; Herchel, R.; Leng, J.-D.; Tong, M.-L. High-spin tetranuclear MnII2MnIV2 clusters with unique Mn(ii)-Mn(iv) magnetic exchange: synthesis, structures and magnetism. *Dalton Trans.* **2009**, 3182.
(51) Buschmann, W. E.; Miller, J. S. Magnetic Ordering and Spin-Glass Behavior in First-Row Transition Metal Hexacyanomanganate-(IV) Prussian Blue Analogues. *Inorg. Chem.* **2000**, *39*, 2411.
(52) Buitendach, B. E.; Erasmus, E.; Niemantsverdriet, J. W.; Swarts, J. C. Properties of Manganese(III) Ferrocenyl-β-Diketonato Complexes Revealed by Charge Transfer and Multiplet Splitting in the Mn 2p and Fe 2p X-Ray Photoelectron Envelopes. *Molecules* **2016**, *21*, 1427.
(53) Fujiwara, M.; Matsushita, T.; Ikeda, S. Evaluation of Mn3s X-ray photoelectron spectroscopy for characterization of manganese complexes. *J. Electron Spectrosc. Relat. Phenom.* **1995**, *74*, 201.
(54) Mansour, A. N.; Melendres, C. A. Characterization of $KNiIO_6$ by XPS. *Surf. Sci. Spectra* **1994**, *3*, 287.
(55) Fuentes, S.; Muñoz, P.; Barraza, N.; Chávez-Ángel, E.; Sotomayor Torres, C. M. Structural characterisation of slightly Fe-doped $SrTiO_3$ grown via a sol-gel hydrothermal synthesis. *J. Sol-Gel Sci. Technol.* **2015**, *75*, 593.
(56) Bressan, M.; Furlani, C.; Polzonetti, G. XPS of coordination compounds: additive ligand effect in some copper(I) and copper(II) chelates with 1,2 phosphino (or phosphine/oxide)-sulfido ethane ligands. *Polyhedron* **1983**, *2*, 523.
(57) Niarchos, D.; Petridis, D. High field Mössbauer effect studies of some anionic iron (IV) dithiochelates. *Chem. Phys.* **1979**, *41*, 97.
(58) Sellmann, D.; Geck, M.; Knoch, F.; Ritter, G.; Dengler, J. Transition-metal complexes with sulfur ligands. 57. Stabilization of high-valent iron(IV) centers and vacant coordination sites by sulfur. pi.-donation: syntheses, x-ray structures, and properties of [Fe-("S2")2(PMe3)n] (n = 1, 2) and (NMe4)[Fe("S2")2(PMe3)-2].CH3OH ("S2"2- = 1,2-benzenedithiolate(2-)). *J. Am. Chem. Soc.* **1991**, *113*, 3819.
(59) Voloshin, Y.; Belaya, I.; Krämer, R. *Cage Metal Complexes: Clathrochelates Revisited*; Springer, 2017.
(60) Novikov, V. V.; Pavlov, A. A.; Belov, A. S.; Vologzhanina, A. V.; Savitsky, A.; Voloshin, Y. Z. Transition Ion Strikes Back: Large Magnetic Susceptibility Anisotropy in Cobalt(II) Clathrochelates. *J. Phys. Chem. Lett.* **2014**, *5*, 3799.
(61) Novikov, V. V.; Pavlov, A. A.; Nelyubina, Y. V.; Boulon, M.-E.; Varzatskii, O. A.; Voloshin, Y. Z.; Winpenny, R. E. P. A Trigonal Prismatic Mononuclear Cobalt(II) Complex Showing Single-Molecule Magnet Behavior. *J. Am. Chem. Soc.* **2015**, *137*, 9792.
(62) Hegetschweiler, K.; Kradolfer, T.; Gramlich, V.; Hancock, R. D. The Design of Selective Chelating Agents: 1,3,5-Trideoxy-1,3,5-tris-(dimethylamino)-cis-inositol, a Powerful Ligand for Hard and Highly Charged Metal Ions. *Chem. - Eur. J.* **1995**, *1*, 74.
(63) Morgenstern, B.; Steinhauser, S.; Hegetschweiler, K.; Garribba, E.; Micera, G.; Sanna, D.; Nagy, L. Complex Formation of Vanadium(IV) with 1,3,5-Triamino-1,3,5-trideoxy-cis-inositol and Related Ligands. *Inorg. Chem.* **2004**, *43*, 3116.
(64) Al Shaer, D.; Al Musaimi, O.; de la Torre, B. G.; Albericio, F. Hydroxamate siderophores: Natural occurrence, chemical synthesis,

https://doi.org/10.1021/acs.inorgchem.0c03362
Inorg. Chem. 2021, 60, 5523−5537

iron binding affinity and use as Trojan horses against pathogens. *Eur. J. Med. Chem.* **2020**, *208*, 112791.
(65) Guérard, F.; Lee, Y.-S.; Tripier, R.; Szajek, L. P.; Deschamps, J. R.; Brechbiel, M. W. Investigation of Zr(IV) and ^{89}Zr(IV) complexation with hydroxamates: progress towards designing a better chelator than desferrioxamine B for immuno-PET imaging. *Chem. Commun.* **2013**, *49*, 1002.
(66) Jones, K. E.; Batchler, K. L.; Zalouk, C.; Valentine, A. M. Ti(IV) and the Siderophore Desferrioxamine B: A Tight Complex Has Biological and Environmental Implications. *Inorg. Chem.* **2017**, *56*, 1264.
(67) Duckworth, O. W.; Bargar, J. R.; Sposito, G. Coupled biogeochemical cycling of iron and manganese as mediated by microbial siderophores. *BioMetals* **2009**, *22*, 605.
(68) Lee, H. B.; Bogart, J. A.; Carroll, P. J.; Schelter, E. J. Structural and electrochemical characterization of a cerium(iv) hydroxamate complex: implications for the beneficiation of light rare earth ores. *Chem. Commun.* **2014**, *50*, 5361.
(69) Buglyó, P.; Culeddu, N.; Kiss, T.; Micera, G.; Sanna, D. Vanadium (IV) and vanadium (V) complexes of deferoxamine B in aqueous solution. *J. Inorg. Biochem.* **1995**, *60*, 45.
(70) Anionic N-oxy-ligands such as deprotonated hydroxylamines, hydroxamic acids, and oximes tend to stabilize high-valent metals, in particular Ni(III), due to the strong s-donor capacity of these ligands. As a consequence of this, nitroxyl ligands (such as TEMPO and TEMPO-H) are known to promote various Cu- and Fe-catalyzed oxidation reactions, e.g., oxidation of alcohols to ketones.
(71) Haugland, M. M.; Lovett, J. E.; Anderson, E. A. Advances in the synthesis of nitroxide radicals for use in biomolecule spin labelling. *Chem. Soc. Rev.* **2018**, *47*, 668.
(72) Walroth, R. C.; Miles, K. C.; Lukens, J. T.; MacMillan, S. N.; Stahl, S. S.; Lancaster, K. M. Electronic Structural Analysis of Copper(II)-TEMPO/ABNO Complexes Provides Evidence for Copper(I)-Oxoammonium Character. *J. Am. Chem. Soc.* **2017**, *139*, 13507.
(73) Kleinlein, C.; Bendelsmith, A. J.; Zheng, S.-L.; Betley, T. A. C-H Activation from Iron(II)-Nitroxido Complexes. *Angew. Chem., Int. Ed.* **2017**, *56*, 12197.
(74) Nguyen, T.-A. D.; Wright, A. M.; Page, J. S.; Wu, G.; Hayton, T. W. Oxidation of Alcohols and Activated Alkanes with Lewis Acid-Activated TEMPO. *Inorg. Chem.* **2014**, *53*, 11377.
(75) Scepaniak, J. J.; Wright, A. M.; Lewis, R. A.; Wu, G.; Hayton, T. W. Tuning the Reactivity of TEMPO by Coordination to a Lewis Acid: Isolation and Reactivity of $MCl_3(\eta^1$-TEMPO) (M = Fe, Al). *J. Am. Chem. Soc.* **2012**, *134*, 19350.
(76) Ahlers, C.; Dickman, M. H. Iron-Mediated Cleavage of Coordinated 1,1,1,5,5,5-Hexafluoropentane-2,4-dione by the 2,2,6,6-Tetramethylpiperidine-1-oxyl Nitroxyl Radical. *Inorg. Chem.* **1998**, *37*, 6337.
(77) Dickman, M. H.; Porter, L. C.; Doedens, R. J. Bis(nitroxyl) adducts of bis(hexafluoroacetylacetonato)manganese(II). Preparation, structures, and magnetic properties. *Inorg. Chem.* **1986**, *25*, 2595.
(78) Dighe, S. U.; Chowdhury, D.; Batra, S. Iron Nitrate/TEMPO: a Superior Homogeneous Catalyst for Oxidation of Primary Alcohols to Nitriles in Air. *Adv. Synth. Catal.* **2014**, *356*, 3892.
(79) Iron, M. A.; Szpilman, A. M. Mechanism of the Copper/TEMPO-Catalyzed Aerobic Oxidation of Alcohols. *Chem. - Eur. J.* **2017**, *23*, 1368.
(80) Hankache, J.; Wenger, O. S. Organic Mixed Valence. *Chem. Rev.* **2011**, *111*, 5138.
(81) Heckmann, A.; Lambert, C. Organic Mixed-Valence Compounds: A Playground for Electrons and Holes. *Angew. Chem., Int. Ed.* **2012**, *51*, 326.
(82) Rintoul, L.; Micallef, A. S.; Bottle, S. E. The vibrational group frequency of the N-O stretching band of nitroxide stable free radicals. *Spectrochim. Acta, Part A* **2008**, *70*, 713.
(83) Niu, P.; Liu, X.; Shen, Z.; Li, M. Electrochemical Performance of ABNO for Oxidation of Secondary Alcohols in Acetonitrile Solution. *Molecules* **2019**, *24*, 100.
(84) Wang, X.; Ma, J.; Song, D.; Shen, Z.; Li, M.; Ma, C. Characterization and Electrocatalytic Activity of Poly (4-thienylacetyl-oxy-2, 2, 6, 6-tetramethylpiperidin-1-yloxy) Prepared by Electrochemical Polymerization. *ECS Electrochem. Lett.* **2014**, *3*, H12.
(85) Caneschi, A.; Gatteschi, D.; Renard, J. P.; Rey, P.; Sessoli, R. Magnetic coupling in zero- and one-dimensional magnetic systems formed by nickel(II) and nitronyl nitroxides. Magnetic phase transition of a ferrimagnetic chain. *Inorg. Chem.* **1989**, *28*, 2940.
(86) Zhang, C.-X.; Liao, D.-Z.; Jiang, Z.-H.; Yan, S.-P.; Zhao, B. Synthesis, crystal structure and magnetic properties of a nickel(II) complex with pyridine-substituted nitronyl nitroxide radicals. *Transition Met. Chem.* **2003**, *28*, 621.
(87) Samolova, E.; Premuzic, D.; Plociennik, S.; Hołynska, M.łg. Bis(benzimidazole) as supramolecular building block in manganese-(IV) chemistry. *J. Mol. Struct.* **2019**, *1176*, 366.
(88) Hou, Z.; Sunderland, C. J.; Nishio, T.; Raymond, K. N. Preorganization of Ferric Alcaligin, Fe_2L_3. The First Structure of a Ferric Dihydroxamate Siderophore. *J. Am. Chem. Soc.* **1996**, *118*, 5148.
(89) Nielsen, A.; Larsen, F. B.; Bond, A. D.; McKenzie, C. J. Regiospecific Ligand Oxygenation in Iron Complexes of a Carboxylate-Containing Ligand Mediated by a Proposed Fe^V-Oxo Species. *Angew. Chem., Int. Ed.* **2006**, *45*, 1602.
(90) Wang, F.; Feng, L.; Dong, S.; Liu, X.; Feng, X. Chiral N,N'-dioxide-iron(iii)-catalyzed asymmetric sulfoxidation with hydrogen peroxide. *Chem. Commun.* **2020**, *56*, 3233.
(91) Wang, Y.; Wu, J. I. C.; Li, Q.; Schleyer, P. v. R. Why Are Some $(CH)_4X_6$ and $(CH_2)_6X_4$ Polyheteroadamantanes So Stable? *Org. Lett.* **2010**, *12*, 1320.
(92) Laube, T. First Crystal Structure Analysis of an Aliphatic Carbocation—Stabilization of the 3,5,7-Trimethyl-1-adamantyl Cation by C-C Hyperconjugation. *Angew. Chem., Int. Ed. Engl.* **1986**, *25*, 349.
(93) Corma, A.; Ródenas, T.; Sabater, M. J. Aerobic oxidation of thiols to disulfides by heterogeneous gold catalysts. *Chem. Sci.* **2012**, *3*, 398.
(94) Fernández-Salas, J. A.; Manzini, S.; Nolan, S. P. Efficient ruthenium-catalysed S-S, S-Si and S-B bond forming reactions. *Chem. Commun.* **2013**, *49*, 5829.
(95) Dhakshinamoorthy, A.; Primo, A.; Esteve-Adell, I.; Alvaro, M.; Garcia, H. Boron Nitride Nanoplatelets as a Solid Radical Initiator for the Aerobic Oxidation of Thiophenol to Diphenyldisulfide. *ChemCatChem* **2015**, *7*, 776.
(96) Patra, A. K.; Dutta, A.; Pramanik, M.; Nandi, M.; Uyama, H.; Bhaumik, A. Synthesis of Hierarchical Mesoporous Mn-MFI Zeolite Nanoparticles: A Unique Architecture of Heterogeneous Catalyst for the Aerobic Oxidation of Thiols to Disulfides. *ChemCatChem* **2014**, *6*, 220.
(97) Dethe, D. H.; Srivastava, A.; Dherange, B. D.; Kumar, B. V. Unsymmetrical Disulfide Synthesis through Photoredox Catalysis. *Adv. Synth. Catal.* **2018**, *360*, 3020.
(98) Jensen, K. A.; Holm, A. Investigations of formaldehyde oxime, its polymers and coordination compounds. I. On the nature of the so-called "triformoxime" and isolation of the authentic trimer, 1,3,5-trihydroxyhexahydro-1,3,5-triazine. *Mater.-Fys. Medd. - K. Dan. Vidensk. Selsk.* **1978**, *40*, 1.
(99) North, J. M.; Achey, R. M.; Dalal, N. S. Low-frequency Raman modes of the single-molecule magnets Mn_{12}-acetate and Fe_8Br_8 and their analogs. *Phys. Rev. B: Condens. Matter Mater. Phys.* **2002**, *66*, 174437.
(100) Duraipandian, S.; Petersen, J. C.; Lassen, M. Authenticity and Concentration Analysis of Extra Virgin Olive Oil Using Spontaneous Raman Spectroscopy and Multivariate Data Analysis. *Appl. Sci.* **2019**, *9*, 2433.
(101) DFT calculation of complex **2**. See section 12.2 in the Supporting Information for details.

https://doi.org/10.1021/acs.inorgchem.0c03362
Inorg. Chem. 2021, 60, 5523−5537

(102) Iranpoor, N.; Firouzabadi, H.; Jamalian, A. Deoxygenation of Sulfoxides and Reductive Coupling of Sulfonyl Chlorides, Sulfinates and Thiosulfonates Using Silphos [$PCl_{3-n}(SiO_2)_n$] as a Heterogeneous Phosphine Reagent. *Synlett* **2005**, *2005*, 1447.

https://doi.org/10.1021/acs.inorgchem.0c03362
Inorg. Chem. 2021, 60, 5523−5537